What is the potential of using Sentinel-1 and Sentinel-2 data to map farmer-led irrigated agriculture with machine learning?

A case study in Central Mozambique

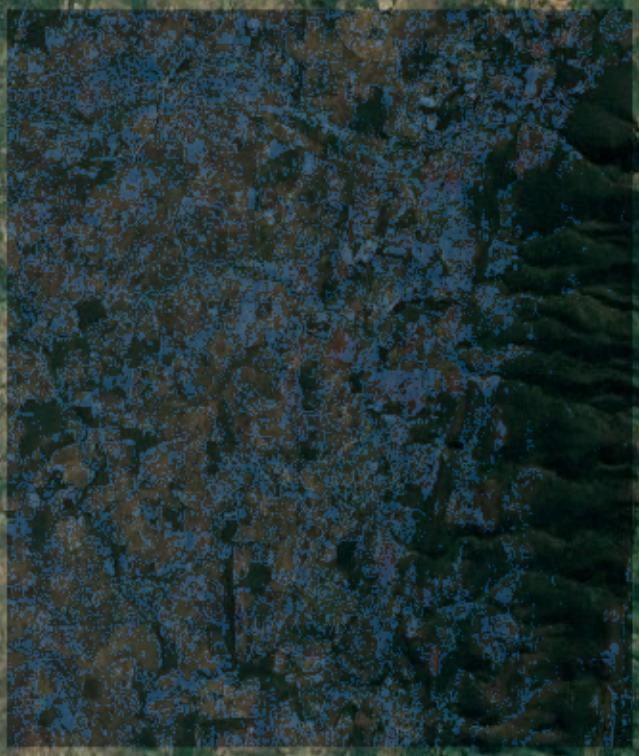

F.M. Crispijn

Delft University of Technology & Resilience B.V.

What is the potential of using Sentinel-1 and Sentinel-2 data to map farmer-led irrigated agriculture with machine learning?

A case study in Central Mozambique

by

F.M. (Floor) Crispijn

to obtain the degree of Master of Science in Civil Engineering
at the Delft University of Technology,
to be defended publicly on Tuesday August 31, 2021 at 12:00 AM.

Student number:	4140737
Thesis committee:	Dr. ir. M.M. Rutten (chair), Water Resources Management
	Prof. dr. ir. S.C. Steele-Dunne, Geosciences and Remote Sensing
	Dr. E. Ragno, Water Resources Management
	Ir. T. Weitkamp, Resilience B.V.

An electronic version of this thesis is available at http://repository.tudelft.nl/.

TU Delft

Summary

Smallholder farmers cultivate more than 75% of the available agricultural land in Africa and therefore this form of agriculture is crucial to the global food supply. At present, little is known about these smallholder agricultural and related irrigation practices, yet the increasing availability and accessibility of remotely sensed data provides significant opportunities to assess the status quo of these practices. However, these characteristic agricultural landscapes can create complexity in identifying land use with the help of remote sensing. The cultivated plots are small and consist of intercropping systems with dynamic spatio-temporal practices concerning planting, irrigation and harvesting.

This research aims to provide insight into the usefulness of remotely sensed passive Sentinel-2 Level-1C and active Sentinel-1 SAR data for land use classification of these complex landscapes with a focus on irrigated agriculture, using a case study in Central Mozambique. For this purpose, an open source-code is written that uses open-source satellite data from Google Earth Engine to execute the supervised image classification methodology, using confusion matrices as an assessment method.

The results of this research appear to show that a nonparametric RF classifier (κ = 88.0%) is preferred over a parametric ML classifier (κ = 85.0%) for processing the data that is high in variability, in which classifications based on the chlorophyll sensitive Red Edge and SWIR bands provide the highest overall accuracies (>88.0%). However, the classifier overestimates the amount of irrigated areas by a factor of 1.5 in the first and a factor of 3 in the second irrigation season. The opportunistic sampling method appears to cause inflated accuracy outcomes and an optimistic bias towards classification of the main class in training. Spectral analysis of the temporal behavior of various S-2 bandwidths does not provide insight into the underlying mechanisms on which the algorithm performs classification. Although it

appears that irrigated agriculture with S-2 data can be identified on the basis of an increase in vegetation biomass and that the classifier benefits from more information through the use of multiple bands.
Research into the use of Sentinel-1 SAR data appears to have potential for identifying irrigation. Time series of the VV backscatter signal show a difference between the irrigation class and the classes non irrigated and light seasonal vegetation in irrigation season 2. However, high standard deviations do reflect the high intra variability of the data, and classification accuracies in this period, do not exceed an overall accuracy of 64.1%. The main confusion as identified by the confusion matrices, comes from classes that are often identified as irrigated, whereas they are not, overestimating the amount of irrigated areas as with the use of S-2 data.

The results of this research show that the used method and data collections do not provide accurate information for the intended classification goal. This research demonstrates in several ways the complexity of supervised image classification in complex agricultural landscapes: the unbalanced and variable reference data of different land uses, which often consist of only a few satellite pixels, make it difficult to identify characteristics of land classes, from which the classifier can derive information. In which Sentinel-1 as added and used in this research, offers no additional insights.

Therefore, in order to improve the identification of farmer-led irrigated agriculture in Manica, other technologies for smart agriculture can be explored in addition to deploying satellite data, such as citizen science. Further research is recommended on the field of using S-1 and S-2 data for classification of complex agricultural landscapes. This may include more advanced methods of performing image classification and accuracy assessement with imbalance datasets, such as: the use of a weighted confusion matrix for accuracy assessment or exploring the use of spatial-spectral instead of pixelwise random forest algorithms. These algorithms seem to be better at handling spatial dependencies and intrinstic heterogeneity which is characteristic of these complex agricultural landscapes. Lastly, it is strongly recommended to assess the use of speckle filters when using SAR data for small target objects. These filters make use of a buffer zone, consisting of a few pixels in size and about the same size of the target object. The main challenge with be to balance the need of speckle reduction and class specific information preservation.

List of acronyms

AI	Artificial Intelligence
CA	Consumer's Accuracy
CART	Classification and Regression Tree
dB	Decibel
DEV	Dense Evergreen Vegetation (LU 3)
GEE	Google Earth Engine
GRD	Ground Range Detected
H	Houses (LU 4)
IF	Irrigated Fields (LU 0)
IR	Infrared band combination: red, near-infrared and shortwave infrared bands: B4, B8, B11, B12
IS-1	Irrigation Season 1
IS-2	Irrigation Season 2
IW	Interferometric Wide swath mode
LC	Land Cover
LSV	Light Seasonal Vegetation (LU 2)
LU	Land Use
LULC	Land Use Land Cover
ML	Machine Learning
NDVI	Normalized Difference Vegetation Index
NIF	Non Irrigated Fields (LU 1)
PA	Producer's Accuracy
R	Rocks (LU 5)

RE	Red Edge band combination: red, near-infrared, shortwave infrared and red-edge bands: B4, B5, B6, B7, B8, B8A, B11, B12.
RF	Random Forest
ROI	Region Of Interest
S-1	Sentinel-1
S-2	Sentinel-2
STD	Standard deviation
SLC	Single Look Complex
SMS	Short Message Service
SVM	Support Vector Machine
VH	Vertical Horizontal polarization
VIS	Visible band combination: visible and near-infrared bands: B2, B3, B4, B8
VV	Vertical Vertical polarization

List of figures & tables

Figure I. Furrow irrigation in the case study area (Hollander, 2018).

1. Introduction

1.1. Background

Forty percent of the food we consume is produced on irrigated land which means that 70 percent of the freswater withdrawals are used for agriculture (Ozdogen et al., 2010). In addition, the world's population has grown from 6.7 billion in 2007 to 7.7 billion in 2019 and is expected to reach almost 10 billion by 2050 (UN World population prospects 2019). The increase in population has already put a great deal of pressure on the current global food and water resources. In the upcoming 30 years, it is expected that the increase in food demand means that 20% more irrigation water is needed (Chakraborty & Newton, 2011; Godfray et al., 2011; Karthikeyan et al., 2020).

Sub Saharan Africa will account for most of the population growth (UN World population prospects 2019). Food supply in this region is mainly provided by smallholder farmers and conducted on a local scale (Funk & Brown, 2009). Together, these smallholder farmers account for more than 50% of the total agricultural sector (Beekman et al., 2014; Burney & Naylor, 2012; De Fraiture & Giordano, 2014). International development policy has recognised this form of agriculture as crucial to achieving the food security objectives sought (Burney & Naylor, 2012; Turral et al., 2011). At present, the extent of smallholder farming in Sub Saharan Africa is mostly unknown. Accurate information on the status quo of these practices are essential for water-resources management regarding food security (Droogers & Aerts, 2005; Vörösmarty & Sahagian, 2000).

The increasing availability and accessibility of remotely sensed data offers significant opportunities to examine the status of smallholder agricultural practices. Remote sensing provides efficient means to monitor agriculture and its related practices at multiple spatial and temporal scales, using either electromagnetic solar radiation

(passive remote sensing) or radiation from the satellite itself (active remote sensing). The objective of this research is to gain more insight into the mapping of smallholder agriculture using remotely sensed data using a case study in Sub Saharan Africa, in Central Mozambique.

Figure 1.1. Channel diverging from small streams, location Manica (Hollander, 2018).

1.2. The case study

The landscape of Central Mozambique consists mainly of farmer-led irrigated agriculture. Hereby, irrigation is initiated and established by the farmer him- or herself, without little or no external support. Cultivated fields are often no larger than 0.2 hectares and irrigation is mainly done by channel diverging from small streams to perform furrow irrigation (figure I). These practices are under rapid development, increase agricultural production and contribute to food security and economic growth in the region. The actual extent of this type of irrigation is currently unknown, due to its informal character (Beekman et al., 2014). The current perception in Central Mozambique is that a large part of the land is not in use and therefore holds potential for agricultural expansion. However, a large part of this land is already in use by smallholder farmers. Therefore, a reliable estimation of the current spatio-temporal extent of this type of agriculture is important to understand and manage the food and water balance (Beekman et al., 2014; Hollander, 2018).

1.3. Previous research

The previous study attempted to identify and map irrigation practices in the area using passive remotely sensed data from the Sentinel-2 satellite. After ground data collection serving as training and validation data, a classification based on images from the first and second irrigation season is performed. This is done with a parametric maximum likelihood classifier, using various combinations of bands and data sets. The results of the classifications of this study are inconsistent, mainly caused by a similar spectral response of irrigated fields and light vegetation. This low inter-class seperability is a result of the heterogeneity and agricultural flexibility of the landscape (Hollander, 2018).

1.4. Knowledge gap

These characteristic landscapes can create complexity in identifying land use. The cultivated plots are small and consist of intercropping systems with dynamic spatio-temporal practices concerning planting, irrigation and harvesting (Bégué et al., 2018; Ozdogen et al., 2010). It is therefore difficult to identify and define the typical characteristics of the different land classes on which the classifications are based. Although common irrigation mapping studies based on passive remote sensing data show promising results, these studies are difficult to transfer to complex areas due to site-specific conditions (Bégué et al., 2018; Ozdogan et al., 2010). In addition, the passive Sentinel-2 product is often hindered by clouds, and therefore crucial information may be missed in order to detect farmer-led irrigated agriculture.

The availability of active remotely sensed data from the Sentinel-1 satellite offers new opportunities to map irrigation under all weather conditions. It can provide a consistent flow of information on vegetation biomass and water content, fundamental indicators of irrigated agriculture. Recently, attempts have been made to create a classification framework for irrigation mapping using active signals, showing promising results (Karthikeyan et al., 2020; Useya & Chen, 2019; Bazzi et al. 2019; Bousbih et al., 2018; Gao et al., 2018). These studies are carried out on large agricultural fields in which monocropping predominates, or on smaller fields that lie in dry landscapes, where there is a big difference between the irrigated agricultural land and the surrounding land covers. This study is conducted in a heterogeneous landscape, with small and dynamic cultivated agricultural fields.

1.5. Research objective

This research aims to get insight in the potential of using Sentinel-1 and Sentinel-2 data to map farmer-led irrigated agriculture with machine learning. For this purpose, a new model is first created to perform the methodological research, using open-source data and an open-source interface. After, this model is compared with the old analysis technique (Hollander, 2018) to which different, non parametric advanced machine learning algorithms are compared to eachother. Last, the possibility of active remotely sensed Sentinel-1 data is examined. This attempts to answer the following sub-questions:

What is the performance of the new model, compared to the old method (Hollander, 2018)

What is the potential of Sentinel-2 data using a Random Forest classifier to identify smallholder irrigation in Manica, Mozambique?

What is the potential of Sentinel-1 data using a Random Forest classifier to identify smallholder irrigation in Manica, Mozambique?

This study is part of an extensive research project concerning farmer-led irrigated agriculture, performed by the Dutch company Resilience B.V., Wageningen University and Research Centre and the national irrigation institute of Mozambique (INIR).

1.6. Outline

Chapter 2, Theory, consists of exploratory research, describing the concept behind the techniques used, based on the literature. Chapter 3, Data and Methods, provides insight in the study area, adresses the systematic and targeted approach for collecting, analysing and interpreting the data and explains the structured methodology to perform the research . Chapter 4. Results, presents the outcome of the study. In chapter 5, Discussion, the key findings of the results are interpreted and explained, as well as the main limitations of this research and the resulting implications. In chapter 6 the main conclusions & recommendations of the study are presented The conclusions answer the research question and the recommendations present how to improve the endproduct for the intended classification goal, and proposals for a new scientific study.

2. Theory

Figure 2.1.
Agricultural development as seen from space: palm trees in Indonesia in 1992 (left) and 2006 (right), retreived from Google Earth.

2.1. Introduction

Of all our five human senses, three work remotely: it is possible to collect information about a target without being in direct contact with it. This concept is widely applied in the field of remote sensing, where satellites are commonly used as a sensor to provide data. Satellite remote sensing uses either electromagnetic radiation from the sun (passive) or radiation from the satellite itself (active). The radiated signals are reflecting, absorbing and transmitting to earth's surface, providing information about the ongoing terrestrial processes at overpass time, for polar satellites. Satellites orbiting the earth can therefore provide a consistent and rich flow of data for multiple applications (Karthikeyan et al, 2020).

One means of converting this data into information is machine learning. Machine learning models are able to learn from prior experiences without being extensively programmed. These models have the potential to evolve into real-time management systems that can handle large amounts of remotely sensed data, and can assist human decision making on a wide range of topics (Virnodkar et al., 2020).

2.2. Agriculture

One of the frequently used applications for remotely sensed data is identifying irrigated agriculture. Irrigation is the partial or complete application of freshwater from surface water bodies and groundwater sources, and needed to compensate for the deficit between potential evaporation, effective precipitation and change in soil moisture content (Ozdogan et al., 2010). The need for water is highly crop specific and irrigated and non-irrigated crops can grow under the same climatic conditions (Ihuoma & Madramootoo, 2017). However, irrigation will provide more active vegetation, resulting in higher degrees of greenness and biomass compared to non irrigated agriculture (Ozdogan et al., 2010). The latter will suffer more water stress and lower the vegetation water content (Agurla et al., 2018). As a result, the natural growing cycle of irrigated and rainfed crops will differ (Pageot et al., 2020).

If these two types of agriculture interact with the satellite signal, the difference in phenology will cause a distinct reflectance (Thenkabail et al., 2005). This is the underlying concept on which irrigation mapping with remote sensing is based, i.e. the difference in reflectance of irrigated areas in relation to non irrigated areas (Karthikeyan et al., 2020).

2.3. Remote sensing

Satellite sensors typically measure the reflected signals of the following spectra: the visible/optical spectrum (0.4-0.7 μm); the infrared spectrum consisting of near infrared (NIR) (0.7-1.3 μm; mid infrared (MIR); (1.3–3.0 μm); thermal infrared (TIR) (3.0–14 μm), and the microwave spectrum (1 mm- 1m) (Karthikeyan et al. 2020).

2.3.1. Passive remote sensing

Methods using passive remotely sensed data for measuring spectral responses from the visual and infrared spectrum are widely used for irrigation mapping. Spectral indices such as the Normalized Difference Vegetation Index (NDVI) are derived from these spectra, and able to reveal healthy vegetation, having the ability to obtain a considerable difference between irrigated and non-irrigated areas (Ambika et al., 2016; Ozdogan et al. 2010). However, these passive remote sensing methods are highly dependent on weather conditions and can solely be attainned with solar radiation. Optical satellite products are therefore severely limited in their use in cloud rich areas. Active low-frequency microwaves from active satellite products do have the ability to penetrate clouds.

2.3.2. Active remote sensing

The availability of active remotely sensed radar data offers therefore new opportunities to map irrigation under all weather conditions (Gao et al. 2018). The independence of solar radiation ensures a consistent flow of information that can be obtained during the day, night and in all weather conditions. Since the microwaves are actively transmitted, it is also known what the radar signal consists of. Complex and changing targets such as vegetation dynamics can be interpreted in relation to this constant signal, which is an additional advantage (Steele-Dunne et al., 2017; Bush & Ulaby 1978). Many recent studies have shown that backscatter data from C-band Sentinel-1 satellite sensors contain much more information about phenology and crop dynamics than is currently being used (Steele-Dunne et al., 2017).

Radiation backscatter exists of active microwave radar signals reflecting back from surfaces. If the signal interferes with vegetation, the reflected backscatter signal consists of several components; from the vegetation itself, the underlying soil and a part due to interactions between its canopy and the subsurface (Ulaby et al., 1996; Kim et al., 2005). How precisely the radar signal interacts with the vegetation is influenced by both the system and its target. The radar is referred to as the system

and obtains information with a certain wavelength and polarization which are transmitted under a particular incident and azimuth angle (Balenzano et al., 2010; Joseph et al., 2010; Ulaby, 1975).

Microwaves interacting with the canopy are affected by the size, shape, orientation, roughness and dielectric properties of individual scatter components, such as leaves and stems, and their distribution throughout the canopy (McDonald et al., 2000; Hoekman & Bouman, 1993; Karam et al., 1992; Yueh et al., 1992; Karam & Fung, 1989; Sarabandi et al., 1988; Senior et al., 1987). Since radar data can provide information on vegetation density and soil moisture, it has great potential to map irrigation targets (Karthikeyan et al., 2020; Bazzi et al. 2019; Useya et al., 2019; Bousbih et al., 2018; Gao et al., 2018).

2.4. Machine learning

Computers can be of assistance to process and interpret both optical and radar data. The information flow from satellites can be delivered to the computer in two forms.
In pixel based methods, data is obtained per grid cell and is then linked to a certain land cover or land use (Vogels, 2019). Another method is object based image analysis, which groups objects or pixels together based on spectral similarities (Blaschke et al., 2014). Machine learning techniques help to classify the unknown pixels.

Within these techniques, a distinction can be made between supervised and unsupervised learning methods (Warner et al., 2009). Supervised methods create a classification of unknown pixels using characteristics of known pixels. These predefined pixels are called classes and are referred to as training data (Cawley & Talbot, 2010). Unsupervised classification groups pixels together based on similar characteristics. These characteristics are not predefined and need to be interpreted after the seperation process (Enderle & Weih, 2005). The computer does not have an intuitive mechanism for segregating information and must therefore apply statistical methods for data seperation, in order to classify different land uses and land covers. The classified land cover map needs to be subjected to accuracy assessment to determine its accuracy. If sufficient, it can be used to obtain a status quo of the area, in order to apply informed decision-making for agricultural water management.

3. Data & Methods

Figure 3.0.1. Manica, in Mozambique, Sub-Saharan Africa, depicted by the white dot.

Introduction

The main method applied in this study is supervised land use classification. Supervised classification consist of five phases: 1. class definition, 2. pre-processing, 3. training, 4. (automated) pixel assignment and 5. accuracy assessment (Warner et al., 2009). First, the study area will be discussed briefly. The data section elaborates on the process of class definition and associated construction of training data. The various satellite products and preparation of their data are defined under satellite data & pre-processing. The methodology is depicted in the conceptual framework in figure 3.0.2. and explains the data collection components and the training, classification and accury assessment steps.

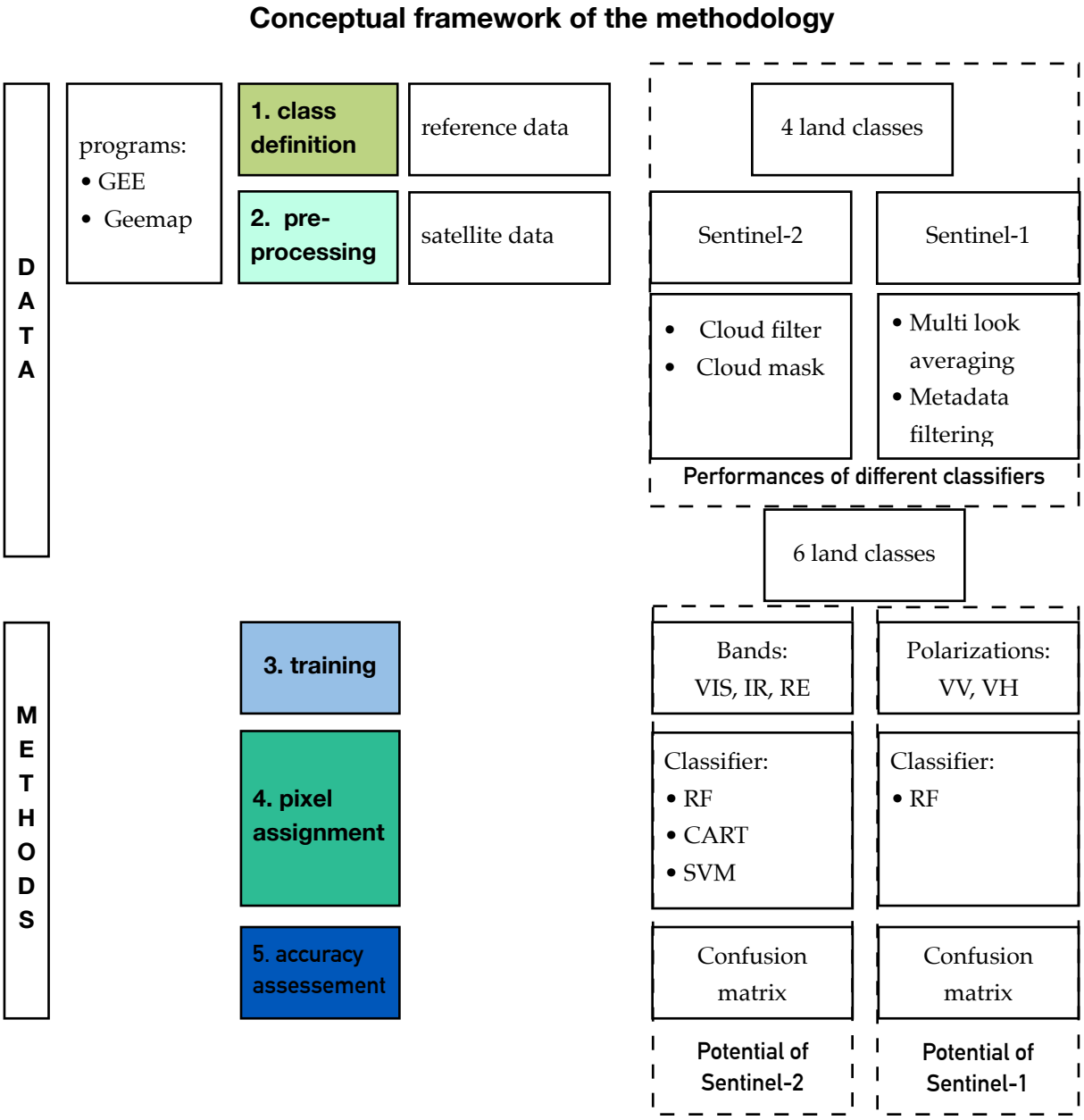

Figure 3.0.2. Conceptual framework of the methodology. The classifiers used are: Support Vector Machine (SVM), Classification and Regression Trees (CART) and Random Forest (RF).

3.1. Study area

This research focuses on a region of interest (ROI) in Manica, a province of Mozambique situated in the central part of the country and bordering Zimbabwe to the west. The total area of Manica is more than 60.000 km^2. In Manica, agriculture is practiced extensively due to the favorable conditions: fertile soils, different microclimates and suitable natural advantages enables the cultivation of a variety of crops. Temperature ranges between 22 to 28 ˚C and precipitation takes place from November to March, and is approximately 800-1000 mm per year (Jansen et al., 2008).

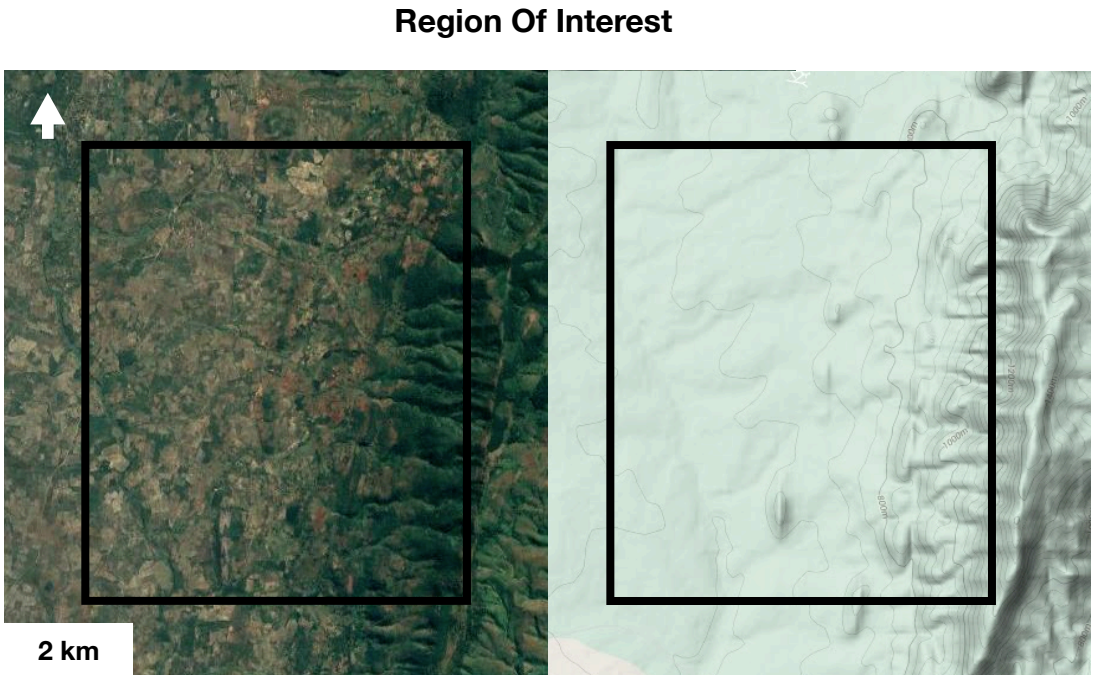

Figure 3.1.1. Illustration of a true color composite and the height map with the overlaying ROI. The area spans from -18.902910289818745 to -18.965261597553866 latitude and 33.09339685375451 to 33.14935846264123 longtitude

3.1.1. Irrigation

The unequal distribution of rainfall results in wet summers and dry winters and influences the planting, cultivating and harvesting of crops. Most crops have a growing cycle of three to four months which allows three agricultural seasons per year. Based on these growing cycles and the amount of rainfall, the following seasons can be distinguished:

The wet season (WS): here, rainfed crops such as sorghum and maize are grown. This period starts at the end of November and lasts till April. The vast majority of

agricultural practices take places during this period.

Irrigation season 1 (IS1): this is the dry season, although there is sufficient water from streams available for the farmers to irrigated their land. This period is approximately from May to July. Agricultural practices are present to a lesser extent than in the wet season, but a large part of the study area is still used for cultivation.

Irrigation season 2 (IS2): a dry season characterised by water scarcity. In general, irrigation is possible in the mid-and upstream part of the area. Downstream, there is often not enough water available for irrigation. This period lasts from August till November. Agricultural activities are present in a lesser extent than irrigation season 1 and the wet season, and mainly limited by the availability of water.

These three different seasons are an approximation. A strict agricultural agenda with fixed planting, harvesting or irrigation periods is non existing. The farmers determine their own schedule, timing differs per season and per field. Agricultural practices are dynamic and flexible, and situations change rapidly (Hollander, 2018; Beekman et al., 2014).

3.1.2. Meteorological data

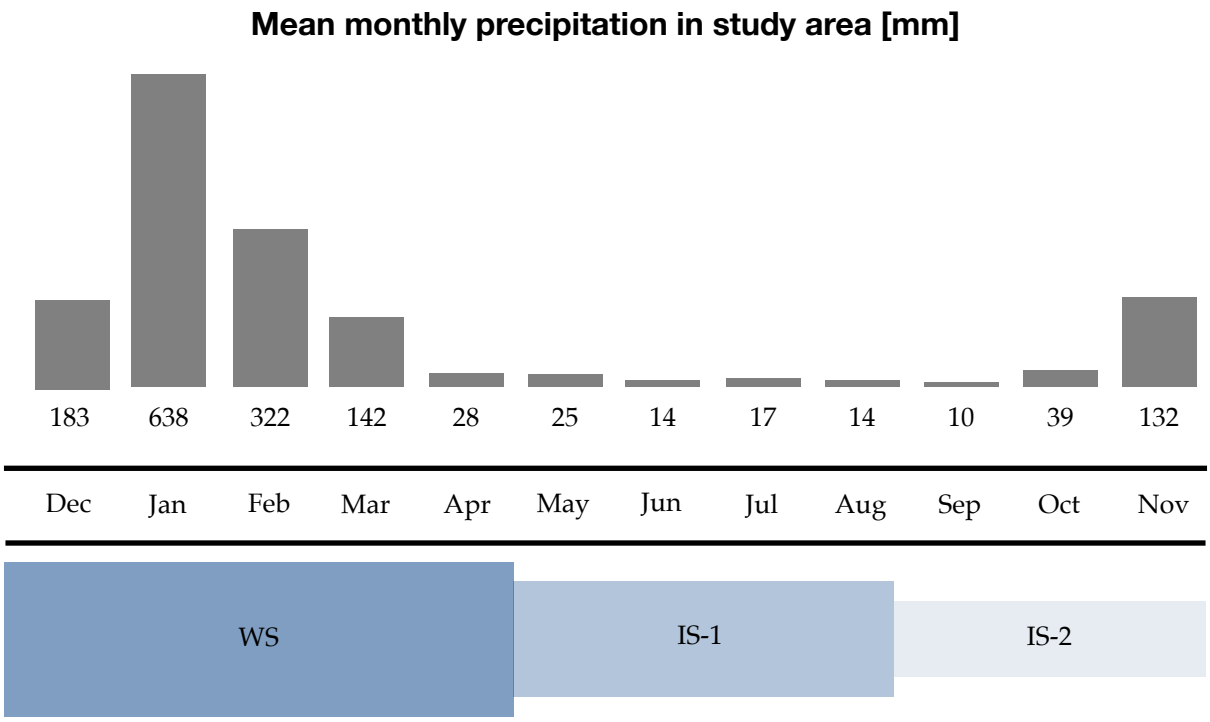

Figure 3.1.2. Mean monthly precipitation in the year 2017 shown in mm. These values are obtained with the CHIRPS pentad data in Google Earth Engine. The WS: wet season, IS-1: irrigation season 1 and IS-2: irrigation season 2, as indicated by (Hollander 2018).

Data

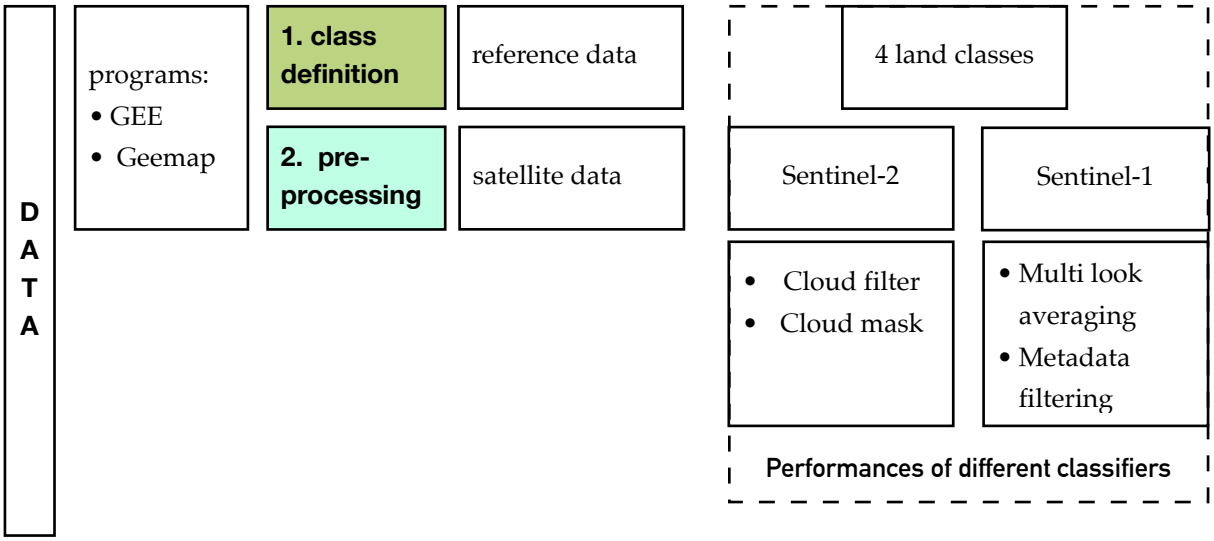
DATA
programs:
• GEE
• Geemap
1. class definition
reference data
2. pre-processing
satellite data
4 land classes
Sentinel-2
Sentinel-1
• Cloud filter
• Cloud mask
• Multi look averaging
• Metadata filtering
Performances of different classifiers


Dense evergreen vegetation

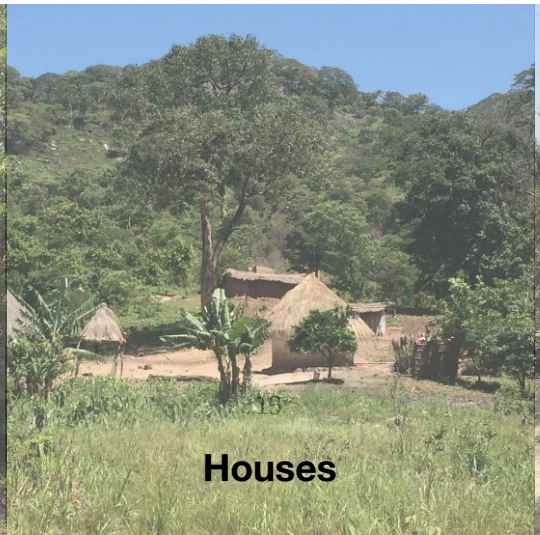
Houses


Rocks

Reference data

1. Class definition

Fieldwork has been executed in the region between 03 October 2017 and 08 December 2017 by (Hollander, 2018). A total of 300 locations were visited with 58 famers interviewed, to obtain expert knowledge about the area and its irrigation practices. The main land covers and land uses that could be identified are rocks, dense evergreen vegetation, houses, irrigated agricultural fields, non-irrigated agricultural fields and light seasonal vegetation. The latter three are dominant in the region and also exhibit phenological similarities.

3.2.1. Training data

The classification goal is to distinguish irrigated land use of smallholder farmers in an area where other land covers are also present. The first step of supervised classification is to identify the different classes and collect a dataset from them, that can be used as training data for the model. A large, high-quality training set is required as input for the algorithm, in order to understand the linkage between pattern and series that cause a specific outcome (Shi et al, 2020). Training data consists of in-situ examples of different land uses and covers and is used to construct knowledge, that will serve as input for the classifier that performs the classification. This study works with secondary training data; land classes have already been identified and collected in a previous study (Hollander, 2018).

The spatial outlines of the land classes are collected to be used as training data in the form of polygons. Collection of these polygons is based on the process of opportunistic sampling, whereby as much data as possible of a certain class is collected. These data are available in shape files that can be imported to the algorithm and prepared for the classification procedure. The data was first imported in QGIS to add a unique value column of each land use, and then imported to Geemap, where the polygons are scaled to the required WGS 84 (EPSG 4326) spatial reference system.

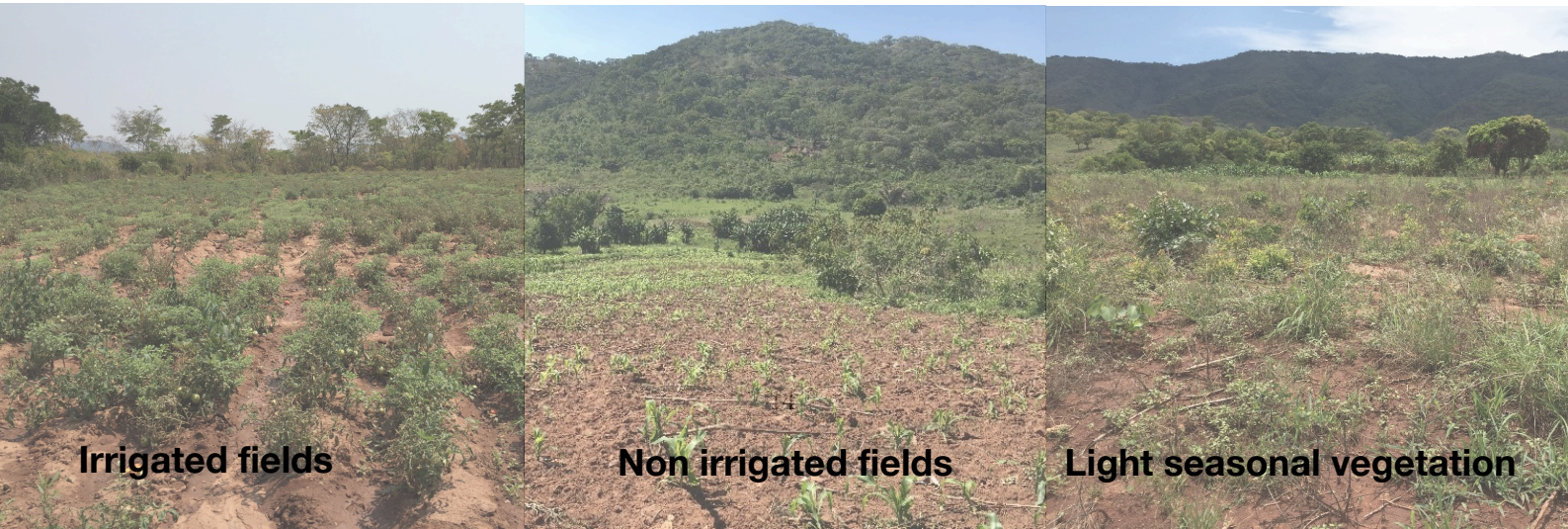

3.2.2. Characteristics of the fields data

The identified land uses and their charactieristics are depicted in figure 3.2.1.:

Land classes and their characteristics

Land class	#	LU	Characteristics
Irrigated fields	146	0	Located near small streams, where irrigation is mainly applied by furrow irrigation. Tomatoes, beans, onions, cabbage and chilies are cultivated in rows.
Non-irrigated fields	30	1	Consist mostly of maize and in a smaller quantity sorghum. Location is not restriced by the presence of an open water body. In the dry season, these areas are often overgrown with natural vegetation.
Light seasonal vegetation	12	2	Shrubs, grasses and small bushes are mostly present in this land class. In the dry season this land class becomes less green and less abundant. A mix of natural vegetation and agriculture is also frequently present.
Dense evergreen vegetation	13	3	Often occurs upstream in the mountains of the study area where the currents originate, or near downstream currents. These land classes retain their vegetation density and greenness all throughout the year.
Houses	28	4	There are no large villages present, only houses clustered in small settlements. These houses and agricultural fields can only be reached via unpaved roads.
Rocks	5	5	A couple of areas in the northern part and some places nearby the ridge consist of permanently bare ground and rocks.

Table 3.2.1. Land classes, amount of class polygons and their characteristic as identified and sampled from 03/10/2017 to 08/12/2017 (Hollander, 2018), each with a unique land use value (LU).

3.2.3. Required spatial and temporal scale

The average size of the irrigated fields used as training data is 0.2 hectares, or 2000 m^2. Polygons of other land covers are not much larger, scattered throughout the area and irregularly shaped. The intra variability in a specific class is high while the inter variability between classes is low: there is no monoculture in terms of crop cultivation. This results in a heterogeneous and therefore complex agricultural landscape, where agricultural and irrigation practices are dynamic and situations change rapidly (Hollander, 2018; Beekman et al., 2014).

As reference, many classification studies with the aim of identifying irrigation have been carried out in desert areas in the United States. These are often center pivots that consist of one type of crop, and, as in this example, covers an area of 550000 m^2 , almost 275 times as much as the average irrigated field in Manica, Mozambique. In addition, the agricultural landscape is designed orderly with a strict cultivation agenda which makes it easy to distinguish land uses (Ozdogan et al., 2010). In order to detect the rapid changes in the small and complex landscape, satellite data with the highest possible spatial and temporal resolution is used.

Complex versus orderly agricultural landscape

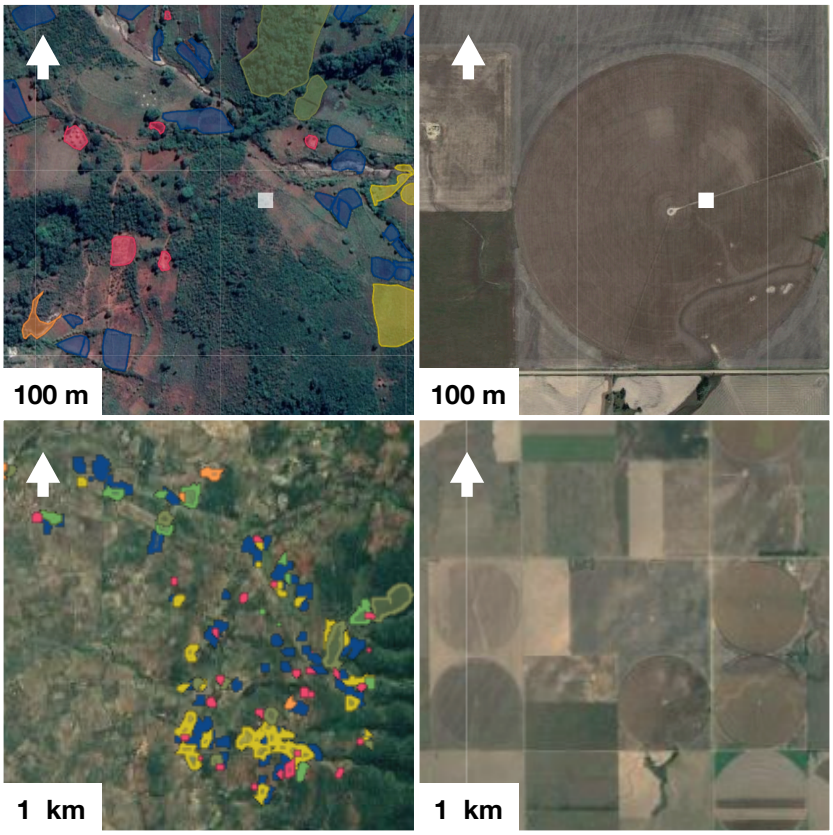

Figure 3.2.2. Polygons of the training data in the research area, compared to a reference study in Kansas, U.S.A. The white square depicts a 10*x*10 m^2 resolution pixel.

Satellite data

2. Pre-processing

The choice of satellites is limited given the spatial and temporal resolution required for the intended classification goal. The Copernicus Program provided by the European Space Agency, which launched the Sentinel-1 (S-1) and Sentinel-2 (S-2) satellite missions in 2014, do meet the requirements.

S-2 is a multispectral instrument consisting of twin polar orbiting satellites moving in the same orbit, phased at 180 degrees to each other. The mission has a revisit time of 5 days at the equator under cloud free conditions. S-2 works with a passive sensor and needs therefore radiation from the sun to obtain information about the earth (ESA, 2013).

S-1 sensors collect data from a dual-polarization C-band Synthetic Aperture Radar (SAR) instrument which operates at a central frequency of 5.405 GHz. The mission is composed of a constellation of two satellites that operate in a sun synchronous, near-polar orbit with a 12-day revisit time each and a 6 day repeat cycle at the equator as constellation. S-1's active sensor can observe earth's surface at any time of the day and night, regardless meteorological conditions (ESA, 2013).

This research makes use of the Sentinel-2 Level-1C orthorectified top-of-atmosphere reflectance data 'ee.ImageCollection("COPERNICUS/S2")' for exploring the performance of different non-parametric machine learning classifiers such as Random Forest. Thereafter, the possibility for Sentinel-1 SAR GRD:
C-band Synthetic Aperture Radar Ground Range Detected, log scaling 'ee.ImageCollection('COPERNICUS/S1_GRD')' data to detect irrigation of smallholder farmers is investigated.

Sentinel-2

3.3.1. Bands

Sentinel-2 data is a multi-spectral imaging instrument that obtains data in a wide-swath, high-resolution mode in 16 different spectral bands that represent that top of atmosphere reflectance scaled by 10000. The name of S-2 bands, its corresponding pixel size and wavelength and description of the band is depicted in table 3.3.1.

Band names, pixel size, wavelength and description of Sentinel-2

	Pixel size [m]	Wavelength [nm] S-2A/S-2B	Description
B1	60	443.9 / 442.3	Aerosols
B2	10	496.6 / 492.1	Blue
B3	10	560 / 559	Green
B4	10	664.5 / 665	Red
B5	20	703.9 / 703.8	Red Edge 1
B6	20	740.2 / 739.1	Red Edge 2
B7	20	782.5 / 779.7	Red Edge 3
B8	10	835.1 /833	NIR
B8A	20	864.8 /864	Red Edge 4
B9	60	945 / 943.2	Water vapor
B10	60	1373.5 /1376.9	Cirrus
B11	20	1613.7 /1610.4	SWIR 1
B12	20	2202.4 / 2185.7	SWIR 2

Table 3.3.1. Name of spectral bands of Sentinel-2, pixel size in meters, wavelength of the S-2A and S-2B in nanometers instruments and descripton of the bands.

Sentinel-2 pre-processing steps

3.3.2. Cloud filter

The signal that optical sensors receive is not able to penetrate through clouds. Therefore, pre-processing of optical data consists of a large part of filtering these clouds and filling information gaps arising from the presence of these clouds. A cloud filter removes images that contain a certain amount of cloud coverage. The threshold of the maximum allowed cloud cover can be set manually. During this research, tests have been carried out using cloud filters with a 5,10,20,40,60 and 80% cloud coverage threshold, to investigate the effect of different threshold values on the amount of output images which led to a choice of 20%.

3.3.3. Cloud mask

The classifier may misidentify the clouds as a particular land class and thereby distort the outcome. A cloud mask will change cloudy pixels in an image to a pixel with 'no-data'. The S-2 collection in GEE has a built-in Quality Assessment (QA) band which contains cloud cover information to apply a cloud-mask. The level-1C mask function uses reflectance threshold from the visible (B1,B2) and SWIR bands (B10, B11 and B12). The function uses an algorithm to create the QA60 band, that is used to remaining dense and cirrus clouds (Coluzzi et al., 2018).

Sentinel-1

3.3.4. Polarization modes

S-1 data is obtained with a number of different instrument modes, resolutions and band combinations in both ascending and descending orbits. The options for the instrument modes are stripmap (S), interferometric wide swath (IW), extra-wide swath (EW) and wave mode (WV). Images can be obtained in either 10, 25 or 40 meter resolutions. The dual polarization SAR system actively transmits microwave signals to the earth with horizontal (H) or vertical (V) polarizations which are then received in both H and V polarizations. This received polarization signal is a portion of the transmitted energy, received by the satellite as backscatter from the ground. The sensor retrieves the backscatter shortly after and at a slightly different location than the emitted signal as the satellite continues its path along the orbit. The phase information and brightness amplitude of the received signal is collected and used to construct an image of the situation on the ground (ESA, 2013). Table 3.3.2. depicts the polarization name, pixel size, wavelength and description of the Sentinel-1 product.

Polarization name, pixel size, wavelength and description of Sentinel-1

	Pixel size [m]	Wl [GHz]	Description
HH	10	5.405	Single co-polarization
HV	10	5.405	Dual-band cross-polarization
VV	10	5.405	Single co-polarization
VH	10	5.405	Dual-band cross-polarization

Table 3.3.2. Band names including polarization modes of Sentinel-1, pixel size in meters, wavelength in gigahertz and descripton of the polarizations.

Sentinel-1 pre-processing steps

3.3.5. Acquisition dates

The Sentinel-1 data is filtered to location and time-period to only obtain images of the Region Of Interest and within 01/01/2017 and 01/01/2018. From this, information is obtained from the time moments as shown in table 3.3.3.

Acquistion dates of Sentinel-1 images

1	2	3	4	5	6	7	8	9	10	11	12
x	21	5	10	4	9	3	8	1	10	12	6
x	x	17	22	16	21	15	20	13	19	24	18
x	x	29	x	28	x	27	x	25	31	x	30

Table 3.3.3. Acquistion dates of Sentinel-1 images, the top represent the number of the month with the corresponding image obtained at that date in the year 2017.

3.3.6. Pre-processing by Google Earth Engine

The Ground Range Detected (GRD) scenes in Google Earth Engine (GEE) are processed to backscatter coefficients (σ^0), in the decibel units (dB). The backscatter shows if the radiated terrain scatters the incident microwave signal primarily towards the sensor (dB > 0) or away (dB < 0) . The retrieved backscatter coefficient is the backscatter area per unit ground area and can vary several orders of magnitude. Therefore the backscatter coefficient (σ^0) is converted to (dB) as $10 * log_{10\sigma^0}$. The intensity of the backscatter is mainly dependent on the physical characteristics of the terrain: the geometry of the target and its electromagnetic properties. The following pre-processing steps have been carried out, applicable to the data used for this research, as implemented by the S-1 toolbox. This, to obtain the backscatter coefficient of each pixel, which may show irrigation and vegetation dynamics:

- Orbit file application: the satellite flying orbit track is detected by many sensors. This step filters the orbit metadata with a restituted orbit to obtain the precise orbit data for improved geocoding.
- Thermal noise removal: for acquisition of scenes in multi-swath modes, this process removes additive noise that appears in sub-swaths in order to decrease discrepancies between these sub-swaths.

- Radiometric calibration: this calibration uses sensor calibration parameters to construct backscatter intensities from GRD metadata.

3.3.7. Metadata filtering

To generate a homogenous subset of S-1 data as used for this research, the collection is also filtered by the following metadata properties:

- Transmitter receiver modes: ['VV'], ['HH'], ['VV' + 'VH'].
- Instrument mode: 'IW' .
- Orbit properties passs: for the ROI, data is only available in 'DESCENDING' mode.
- Resolution in meters: as the target has narrow dimensions, the highest resolution of 10 meters is chosen.
- Resolution High or Medium: the selected pixel spacing of 10 meters and Interferometric Wide Swath mode corresponds to a 'H' (High) resolution of level-1C GRD scenes (ESA, 2013).

3.3.8. Speckle filtering

One of the difficulties in handling SAR data is the presence of speckle effects that make visual interpretation challenging. In pictures, the speckle effect appears as random noise but is in fact a consequence of the coherent nature of the radar signal. To reduce this effect, various filters can be applied such as the Frost filter, a Median filter and a Refined lee filter.

GEE uses multi look images. Multi-look processing is done by averaging adjacent pixels for the purpose of reducing the effect of speckle and to compress the data. As these images are already suitable for achieving the intended effect of reducing speckle, this study does not use an additional filter. Another motivation for this decision is that most filters make use of a buffer zone that include the surrounding behaviour of the pixel in determining the pixels' backscatter intensity. In view of the small area to be irrigated, this additional buffer zone may contain information that is incorrectly attributed to a particular class and therefore only complicates the process.

Methods

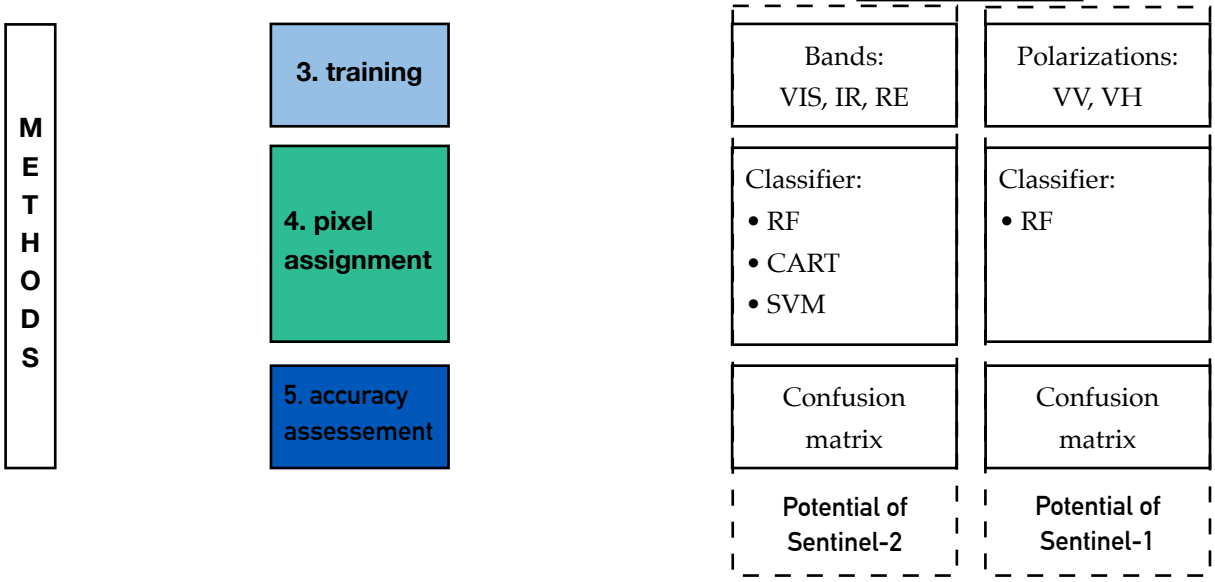
METHODS
3. training
4. pixel assignment
5. accuracy assessement
6 land classes
Bands: VIS, IR, RE
Polarizations: VV, VH
Classifier:
• RF
• CART
• SVM
Classifier:
• RF
Confusion matrix
Confusion matrix
Potential of Sentinel-2
Potential of Sentinel-1

Methods

After the class definition and pre-processing steps have been carried out, these components have been kept constant for the rest of the study.

Performances of different classifiers

This research works with open source GEE data and the open source Python based interface Geemap. No specific affordable or downloadable software is required which is useful for the final product to be delivered. The self-written code is used as a model and capable of performing all the desired calculations. Table 3.4.1. shows the main similarities and differences between the other analysis method (Hollander, 2018) and the new model. The main differences are the number of images obtained and the classifiers used.

3.4. Machine learning methods

3.4.1. Maximum likelihood

Digital image classification algorithms may use parametric conditions based on a normal distributions of the data, nonparametric conditions which does not assume normal data distributions, and nonmetric conditions (Timothy et al., 2009). The previous study (Hollander, 2018) uses a maximum likelihood classifier, which assumes that the statistics of the land classes are normally distributed. This algorithm constructs equiprobability contours around the statistical means of the land classes, and assigns unknown pixels to a class with the highest probability, based on their placement in the contours (Lavender & Lavender, 2015). The examined classifiers used for this study are all nonparametric.

3.4.2. Classification and Regression Trees (CART)

Decision trees are a commonly used algorithm for predictive modeling with machine learning. A decision trees can be depicted as an upside down tree where the roots show the start of the process. The leaves represent specific classes, and the branches the relationship between the characteristics of that class. The decision tree takes the entire package of information from the training set as input; applies several cut-offs in terms of node-splitting based on certain criteria; and continious this process until the branch of the tree is reached; where it generates an output. Classification trees are predicting a discrete class and thus generate a categorical output. Regression trees are used for predicting a continuous quantity to construct a numerical output. Disadvantage of this classifier is that it is relatively sensitive to overfitting.

Similarities and differences between the old method and new model

	WI [GHz]	Other analysis methods (Hollander, 2018)		New model	
Classes	Amount	4		4	
	Irrigated fields	142		146	
	Non-irrigated fields	0		0	
Number of polygons	Light seasonal vegetation	20		13	
	Dense evergreen vegetation	25		12	
	Houses and rocks	32		33	
	Total	219		204	
Data And Pre-processing	Data	Sentinel-2 TOA		Sentinel-2 TOA	
	Data provider	Copernicus open acces hub		Google Earth Engine	
	Pre-processing	Sen2Cor		Google Earth Engine	
	Program	QGIS & GRASS		GEEmap	
Images obtained	Irrigation season 1	08/06/2017	13/06/2017	08/06/2017	13/06/2017
		28/06/2017	23/07/2017	28/06/2017	23/07/2017
	Irrigation season 2	17/08/2017		17/08/2017	22/08/2017
				27/08/2017	01/09/2017
				06/09/2017	11/09/2017
			26/09/2017	16/09/2017	26/09/2017
		01/10/2017		01/10/2017	06/10/2017
		11/10/2017	16/10/2017		16/10/2017
		26/10/2017	20/11/2017	26/10/2017	20/11/2017
	Aggregation	Mosaic		Mosaic	
Bands	VIS	2, 3, 4, 8		2, 3, 4, 8	
	IR	4, 8, 11, 12		4, 8, 11, 12	
	RE	4, 5, 6, 7, 8, 8A, 11, 12		4, 5, 6, 7, 8, 8A, 11, 12	
Classifier	Machine learning method	Maximum likelihood		CART	
				Random Forest	
				Support Vector Machine	
Accuracy	Training / testing [%]	80	20	80	20

Table 3.4.1. Similarities and differences between the old and new method (Hollander, 2018)

Overfitting occurs when the model learns from outliers and noise in the training data to such an extent that is negatively affects its accuracy in adding new data. Training sets with low variability between the classes might be less suitable for this classifier, due to its inability to discriminate between marginal cases. Datasets with high variability are also less effective for training the classifiers.

3.4.3. Random forest

Random forest is an algorithm that is constructed from an ensemble of decision trees, applicable to both classification and regression. The design of RF is nearly the same as CART, though RF takes only a subset of the available data as input. During node-splitting, RF searches for the best feature to distinguish a key indicator of a specific class, among the random subset of features, instead of searching for the most important feature. Many decision trees can be constructed from different random subsets of data. To construct a final output, the RF assembles the output from all the decision trees in the forest to make a prediction. The addition of randomness in an RF makes the model more robust and less prone to overfitting than CART algorithms. The adverse effect is the complication of interpretation. What happens during the construction of different trees is not simple to determine, which complicates the interpretation and explanation of the model outcomes.

3.4.4. Support vector machine

The goal of the SVM is to construct a hyperplane in an N dimensional space, whereby N depicts he number of features, that seperates the data points. Many hyperplanes can be constructed, but the objective is to find a hyperplane that has the maximum distance between data points of two classes, in case of a two dimensional space. The hyperplane operates as a decision boundary for new data points. Data points falling on a certain side can be attributed to a class, if there are only two distinguishable classes and data characteristics are unfamiliar.

3.5. Accuracy assessment

Since each machine learning method has its own way of separating the training data and classifying new pixels, the final classification maps will also differ. Qualitative analysis can be performed with the classification map produced. To evaluate the performance of the model quantitatively, accuracy assessment is performed. This not only gives insight in the overall performance, it also exposes the underlying

mechanisms of the model. This will help to identify which field characteristics, in combination with the model used, influence the final results.

3.5.1. Confusion matrix

There are various methods to assess the quality of the classification. One of the most commonly used methods is accuracy assessment via a confusion matrix. The confusion matrix shows how the classification model is confused when making predictions. Table 3.5.1. shows an example of a confusion matrix, that calculates the following statistics:

Confusion matrix example

	0	1	2	PA%
0	1682	5	1	99.6
1	39	1542	8	97.0
2	1	35	581	94.1
UA%	97.7	97.3	98.1	**OA%**

Table 3.5.1. example of a confusion matrix consisting of 3 classes.

- **OA**: the overall accuracy = (# pixels correctly classified) / (total # of pixels) and shows the percentage of correctly classified points. This number adds the classified pixels in the main diagonal and divides them through the total amount of pixels, to obtain a value in %.
- **PA**: the producers accuracy (irrigation) = (# of pixels correctly classified a irrigation) / (# ground reference pixels of irrigation). This accuracy evaluates the classification accuracy from the producer's point of view, the mapmaker. This is related to the **Omission Error** = 1- producers accuracy and portrays the number of times a pixel should have been included in that specific class. This is the sum of pixels in a column, the main diagonal exluded.
- **UA**: the users accuracy (irrgation) = (# of pixels correctly classified as irrigation) / (total # of pixels classified as irrigation). This value indicates the classification

accuracy from the user's point of view, the mapviewer. The outcome represents the probability of a pixel that is being classified into a class that is actually that pixel. From this, the **Comission Error** can be calculated as 1 - users accuracy. This represents the number of times that a pixel of a class is included, when it should be excluded. It is the sum within a row without the main diagonal.

3.5.2. Kappa coefficient

The kappa coefficient, or κ is a number that represents the relative performance of the classification, compared to a random classification. It is therefore a reliable way to determine the accuracy of the analysis, since it take into account the probability of a truthful result based on chance. In the field of image classification, κ ranges from 0 to 1 in general, where an outcome of 1 depicts a perfect classification. A zero shows that the outcome is no better than a random classification

3.5.3. Training and testing set

After generation of the training set, it is divided into two datasets: one for training the model and one for accuracy assessment. The training dataset is used to construct a confusion matrix indicating the training accuracy, which gives and indication of the generalization error. With the validation or testing subset, the confusion matrix is created that depicts the testing accuracy. A large difference in testing and training accuracy indicates that the model is prone to overfitting. The classifications were performed with a fixed split of 80% training and 20% testing as in the previous research (Hollander, 2018). To evaluate the robustness of the model, experiments were conducted with different ratios and subsets of training and testing.

3.6. Irrigation estimation

The final classification map shows the distribution of the predicted irrigation, and the accuracy assessment an indication of its validity. Following this, the amount of irrigation can be determined by counting the amount of pixels per prediction. This contributes to the intended classification goal of identifying and quantifying smallholder irrigation in Manica, Mozambique. To compare the different classification methods qualitatively, the different classification maps can be compared to reference images of the area from 12/31/2017, provided by Google Earth Pro. This allows for qualitative assessment of whether the maps obtained are truthful in terms of quantity and distribution of classified land covers.

3.7. Spectral analysis of Sentinel-2

The non-paramatric classifiers group the land classes based on differences and similarities in spectral responses. Analysis of these responses can provide insight into the model's classification process, as well as their usability to identify irrigation. It examines how the classes respond to different bands and indices, in order to extract a specific irrigation signal. In addition, the mean and standard deviation can determine the degree of variability within and between classes. This provides an indication of the quality of the training data set, and therefore the reliability of the classification outcome. This research makes use of the same combination of bands as used in the previous study, based on the frequently used combinations as depicted in table 3.7.1.

Frequently used spectral band combinations for agriculture

Name	B	Sensitivity
Color infrared	**B3 B4 B8**	This band combination places emphasis on vegetation health. The near-infrared band 8 in particular is sensitive to chlorophyll, and therefore dense vegetation will show up red in a color infrared, and urban areas in white.
Short wave infrared	**B12 B8A B4**	In using this combination of shortwave infrared, near-infrared and red-edge, vegetation appears in different shades of green. Dense vegetation is generally characterized by darker shades of green and brown colors indicate rocks and urban areas.
Agriculture	**B11 B8 B2**	This band combination of shortwave infrared, near-infrared and blue is also used for observing vegetation health. B11 and B8A are mainly suitable for indicating dense vegetation, that appears in darker shades of green.

Table 3.7.1. The frequently used spectral bands are depicted in the table, on which the band combinations of this research are based, namely: Visible (VIS), visible and near-infrared bands: B2, B3, B4, B8. Infrared (IR), red, near-infrared and shortwave infrared bands: B4, B8, B11, B12. Red-edge (RE), red, near-infrared, shortwave infrared and red-edge bands: B4, B5, B6, B7, B8, B8A, B11, B12.

The steps described so far carry out the quality control of the new model. It shows how well the three non parametric classifiers are able to make an accurate prediction of new pixels, based on the same three band combinations and two time periods as

in the previous study. This supports the choice of the non-parametric classifier with which to proceed. The sensitivity of the model is determined by testing different ratios and subsets of training and validation data. Next, the six classifications produced are analyzed both qualitatively and quantitatively. The classification map s give an indication of the distribution of the different land uses. In addition, the percentages of these land uses reflect the size of a predicted class. Spectral analysis of various band combinations and indices provide insight into the model's classification process. Finally, it determines how irrigation can best be seen in this training data , using S-2 data.

3.8. The potential of Sentinel-1 data

This study attempts to reduce the problem of low inter-class spectral separability as indicated before (Hollander, 2018) by using ingenious non-parametric machine learning techniques for classification. The problem is caused in particular by the similarity between irrigated fields and light seasonal vegetation on field scale. It is examined whether S-1 SAR data is able to provide additional insight into the temporal behavior of these, and other land uses. This, to potentially add additional information to the model , or create a new model based solely on S-1 SAR data.

3.8.1. Aggregation method

Sentinel-2 data allows spectral signatures of vegetation to be seen. SAR interacts with the land cover and land use through the polarization signals that the product emits. In contrast to S-2 data, there is an important difference with S-1 data. The backscatter intensity of the different polarizations of the SAR data is expressed in a logarithmic scale [dB]. Therefore, the temporal statistics of S-1 are not fully consistent with the mathematical average and standard deviation of the linearly scaled S-2 data. To be able to compare the temporal statistics of the spectral responses and backscatter intensities of different land classes, expressing the standard deviation and mean of both datasets have been used. To construct this figure, it is examined how a difference in aggregation method affects the temporal statistics. For this purpose, boxplots were made based on a mean and median aggregation method. From this it can be seen how the aggregation method influences the minimum, first quartile, median, third quartile, and maximum of the VV and VH polarization in interaction with the land classes. After this, a choice can be made, which aggregation method can best be used for this dataset.

3.8.2. Intra and inter class variability

By investigating the mean and standard deviation of the interaction of the VV and VH polarizations with the different land uses over time, both the intra and inter class variability are examined.

3.8.3. Accuracy assessment

The testing and training data of the classifications of the VV and VH polarizations have been assessed in further detail, in order to understand different mechanisms behind the model.

3.8.4. Influence of different training sets

To see if and how this could possibly cause confusion, a number of new training sets are created where the accuracies are compared to those of a classification with all land classes. A subset is created that includes only the 42 largest irrigation polygons. In addition, another set was created with only the classes irrigated, non irrigated, light seasonal vegetation and dense evergreen vegetation. Finally, a classification was done based on the large irrigated fields, and excluding non irrigation.

4. Results

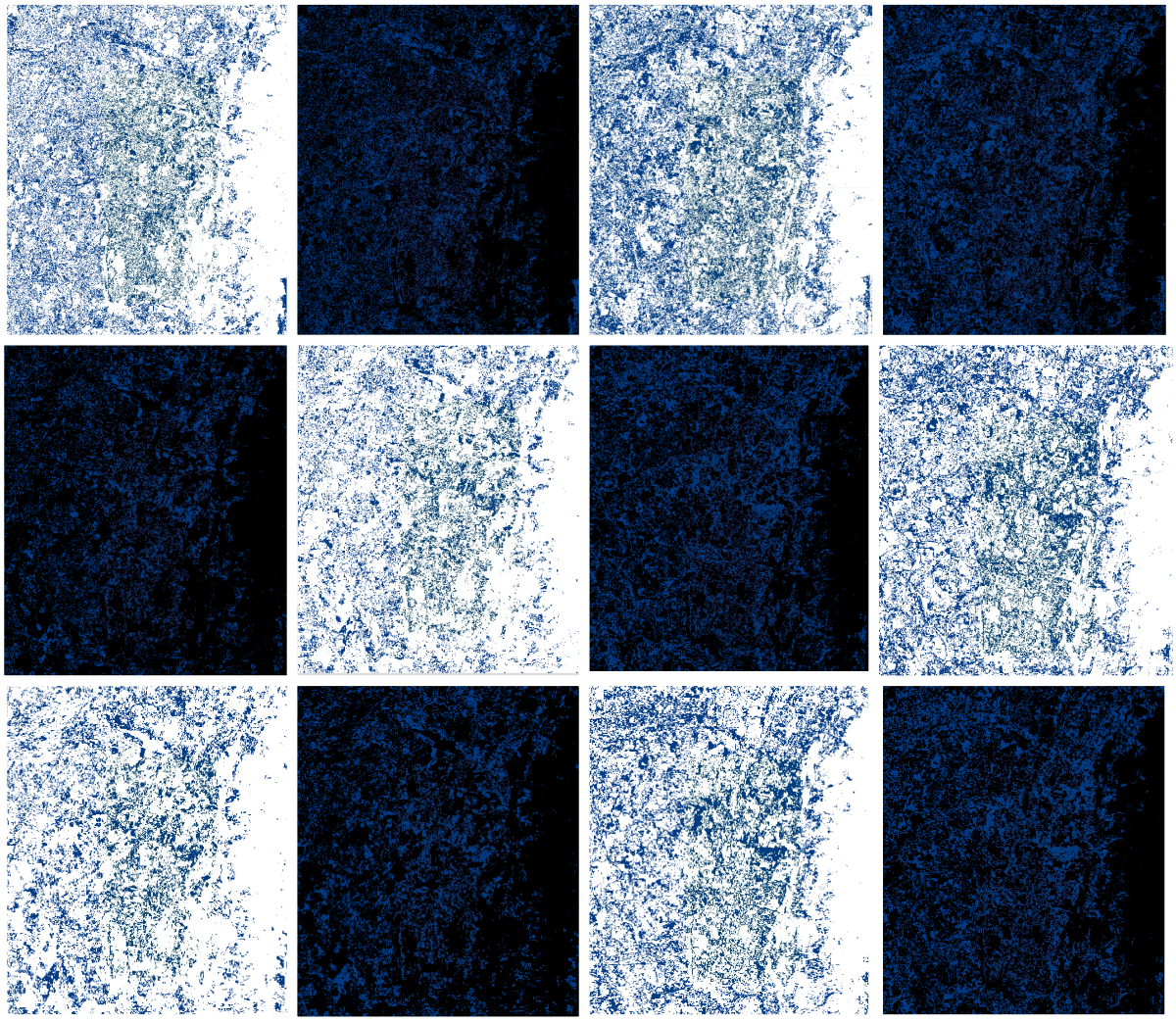

Figure 4.1.1. Illustrative image of predicted amount of irrigated areas, based on VIS, IR, and RE bands in IS-1 and IS-2. From left to right and top to bottom: VIS IS-1, VIS IS-1, VIS IS-2, VIS IS-2, IR IS-1, IR IS-1, IR IS-2, IR IS-2, RE IS-1, RE IS-1, RE IS-2, RE IS-2

4.1. Introduction

This chapter shows the main results which are relevant to the research questions. First of all, the performances of the new model compared to the previous study (Hollander, 2018) are presented. This, along with the performances of different non-parametric machine learning techniques. The potential of both Sentinel-2 and Sentinel-1 data to identify irrigated agriculture in Manica is then discussed.

4.2. Performances of different classifiers

To compare the performances of the old with the new model, the κ accuracies of the six classifications are shown in table 4.2.1. The κ gives an objective estimate of the model performance and the reability of its outcome. The number, on a scale from 0 to 1, represents how well the classification corresponds to the ground data, split from the training subset for validation. The κ indices are calculated from the validation subset. The values from the new model, represent the average outcome based on a 10-fold cross validation.

Kappa accuracies of the old analysis method (Hollander, 2018) and the new model

		New		
	κ ML	κ SVM	κ CART	κ RF
VIS IS1	0.62	0.45	0.53	0.63
VIS IS2	0.85	x	0.54	0.66
IR IS1	0.59	0.43	0.70	0.77
IR IS2	0.80	0.26	0.64	0.74
RE IS1	0.60	0.44	0.81	0.87
RE IS2	0.79	0.32	0.79	0.88

Table 4.2.1. Comparison of kappa accuracies of the old analysis method (Hollander, 2018) and the new model. The κ indices are calculated from the validation subset. The values from the new model, represent the average outcome of a 10-fold cross validation. Based on a classification of 4 different land classes containing 204 polygons. Data is based on Sentinel-2 data in IS-1 and IS-2 using VIS, IR, and RE bands and a 80%/20 % split in training and validation data.

4.2.1. Maximum likelihood

Section 3.5.2. explains that the closer the κ approaches 1, the better the classification succeeded according to the accuracy assessment. The kappas obtained from the maximum likelihood classification of the previous study show the highest values for all band combinations in the second irrigation season. Respectively: 0.23 for the visual band combination, 0.21 for the infrared band combination and 0.19 for the red-edge band combination. The highest accuracy is achieved through the visual band combination in irrigation season 2 with a κ of 0.85.

4.2.2. Support vector machine

Examing the kappas of the new model, it is noticeable that the outcomes of the SVM classification are significantly lower than those classifications with other classifiers. They all do not exceed 0.45. Section 3.4.4. describes that the SVM classifier seperates the data points by means of a constructed hyperplane. However, the model is not able to construct multiple hyperplanes and therefore distinguishes between more than two classes. Because this model wants to predict 4 classes, this could be a cause of the low scores.

4.2.3. Classification and Regression Trees and Random Forest

The κ accuracies of the CART and RF classification methods show much higher κ values than those of the SVM. Outcomes between 0.53 and 0.88 are achieved and in each case, the RF scores between 0.12 and 0.06 are higher than the CART. Both of these machine learning techniques are based on the same decision tree principle, but the RF has a more advanced way of predicting based on building multiple trees.

In contrast to the previous study, the CART and RF classification results do not always show higher outcomes in the second irrigation season. Here, the selection of band combinations is more related to a higher outcome than irrigation season. For both CART and RF, the highest results are obtained in both irrigation seasons with the RE band combination. Then comes the IR combination and finally the VIS band combination. These red bands are sensitive to greenness, which could be an indicator for vegetation biomass. As it seems, the new model can distinguish the classes based on this information.

Since the random forest classifier is the only technique to reach the USGS standard limit of 85%, further research with this classifier is continued.

4.3. Irrigation estimation

The κ accuracies in table 4.3.1. give an indication of the model performance, based on four land uses, three different band combinations and two irrigation seasons. Table 4.3.1. shows the predicted amount of irrigated areas per classification in percentage. The amount of predicted irrigated area by the new model is based on six land uses.

Regarding the amount of predicted irrigated area, the only corresponding value between the old and the new method is that of 33% percent of the RE IS-2. In the first irrigation season the values are also close, they differ by only 1% at this band combination. The other band combinations show no corresponding outcomes. In IS-1, the new model predicts almost 3x more irrigated area for the VIS combination, and almost 2x more for the IR classification. In the IS-2 the predictions of the VIS and IR band combinations from the new model are both 1,3 higher. During fieldwork, it was identified that approximately 10-15% of the total area was irrigated. The new model overestimates this amount in all classifications. The estimated irrigated area of 16% based on the RE bands in IS-1 corresponds most to the situation on the ground.

Predicted irrigated area per classification, old versus new model [%]

	Old	New
VIS-IS1	8	23
VIS-IS2	27	35
IR-IS1	9	17
IR-IS2	26	34
RE-IS1	15	16
RE-IS2	33	33

Table 4.3.1. shows the predicted amount of irrigated areas per classification in %, for the old analysis method (Hollander, 2018) and the new model. The old technique used the 4 land classes: irrigated fields, light seasonal vegetation, dense evergreen vegetation and bare ground and houses. The new model uses the 6 land classes: irrigated fields, non irrigated fields, light seasonal vegetation, dense evergreen vegetation, houses, and rocks. Data is based on Sentinel-2 data in Irrigation season 1 (08/06/2017 to 23/07/2017) and Irrigation season 2 (17/08/2017 to 20/11/2017) and visible (VIS: 2,3,4,8), infrared (IR: 4,8,11,12) and red-edge (RE: 4,5,6,7,8,8A,11,12) band with a 80%/20 % split in training and validation data.

4.4. Outcomes of different classifications

To analyze the results quantitatively, the classification maps are reviewed to evaluate how well the prediction matches the ground situation. The following sections show the predicted quantity and distribution of 6 land uses, based on 6 classifcations, from 2 irrigation seasons using 3 different band combinations.

4.4.1. VIS IS-1

The dominant land use in this area is dark evergreen vegetation, mainly presented at the ridge, and in smaller quantities through the remaining area. This seems to be a good reflection of the situation on the ground in both quantity and location. The positioning of the light seasonal vegetation also seems realistic, especially on the ridge, where it follows the tributaries of the catchment. This prediction indicates that about 28% of the area consists of non irrigated fields. This percentage appears quite high, and it is fragmented throughout the area, not presentable for the ground situation. The predicted irrigation does seem to match the irrigated fields used as training data. However, the classified percentage appears to be overestimated.

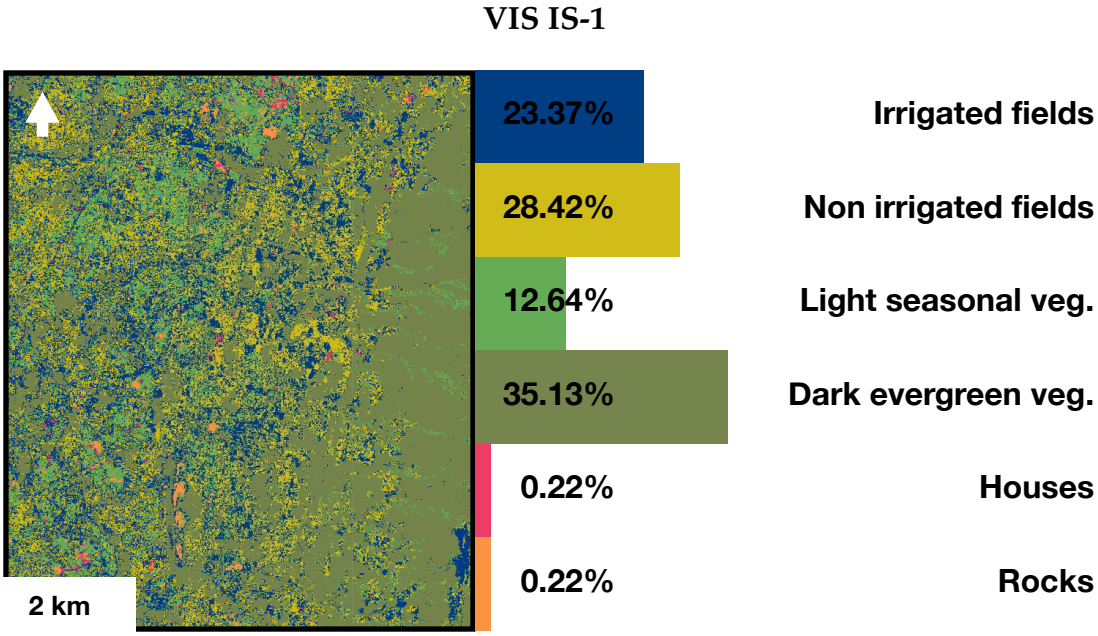

Figure 4.4.1. Classification map showing estimated land use for the visual (VIS: 2,3,4,8) band combination in irrigation season 1 (08/06/2017 to 23/07/2017).

4.4.2. IR IS-1

From this prediction, the vast majority of the area consists of dark evergreen vegetation and non irrigated fields. Mainly the amount of non-irrigated area seems rather over-classified and often seems to be confused with light seasonal vegetation.

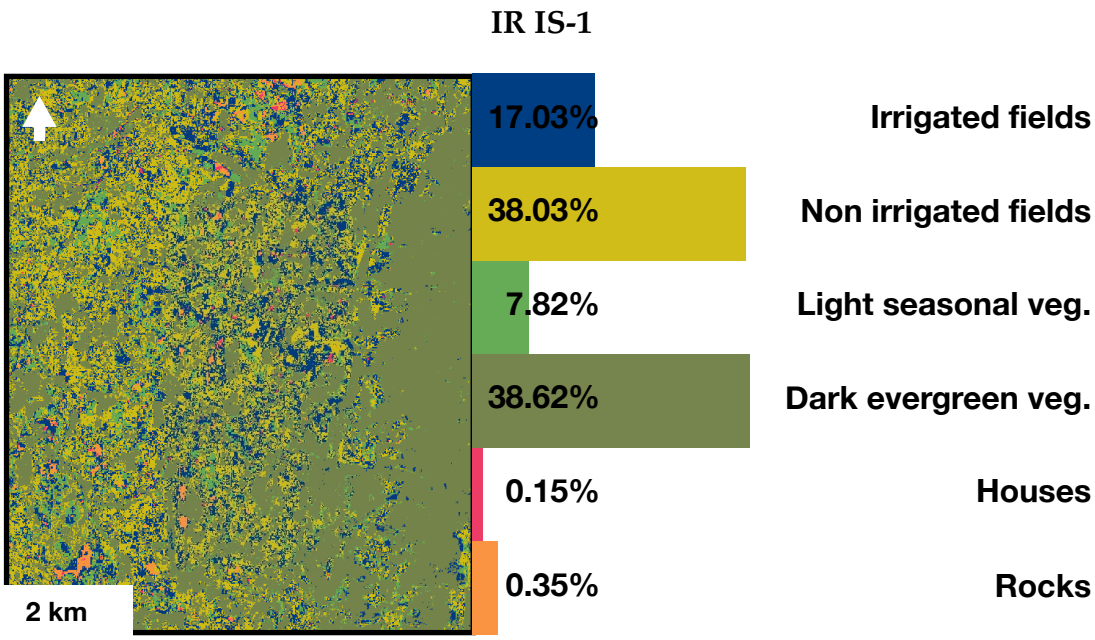

Figure 4.4.2. Classification map showing estimated land use for the infrared (IR: 4,8,11,12 band combination in irrigation season 1 (08/06/2017 to 23/07/2017).

4.4.3. RE IS-1

This classification exhibits similar outcomes both in quantity and distribution as that of IR in IS-2, it also shows dark evergreen vegetation and non irrigated fields as dominant land classes. However, this RE prediction shows the irrigated fields more

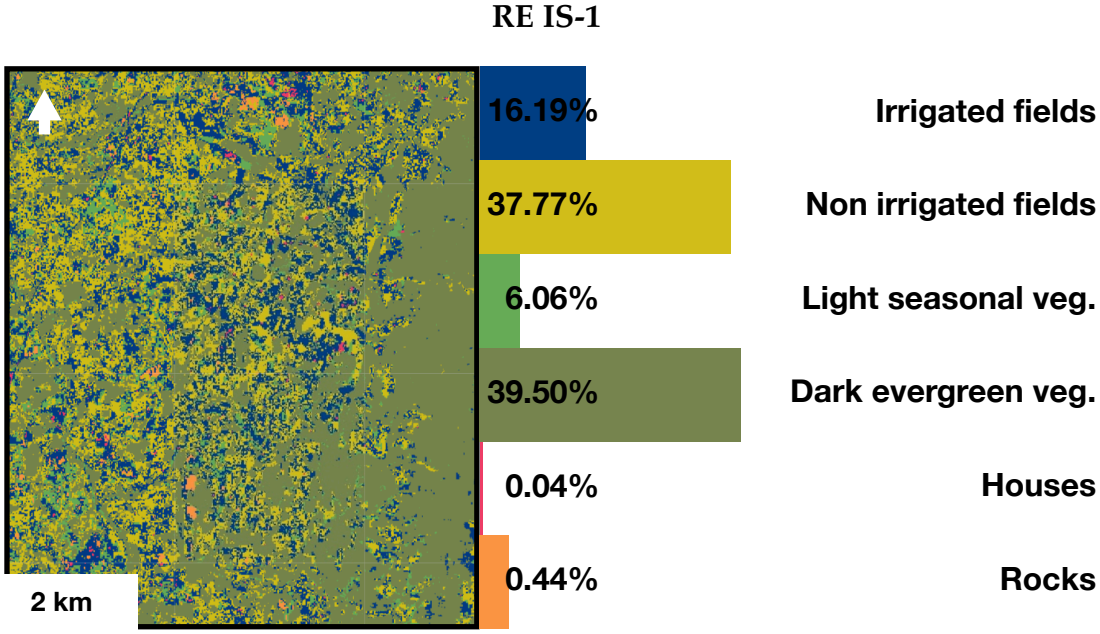

Figure 4.4.3. Classification map showing estimated land use for the red-edge (RE: 4,5,6,7,8,8A,11,12) band combination in irrigation season 1 (08/06/2017 to 23/07/2017).

clustered in the landscape. Also, this band combination classifies irrigated fields, where that of IR classifies this as houses or rocks. This can be seen mainly at the top of the area, and at the bottom left.

4.4.4. VIS IS-2

In the second irrigation season, the main predicted land use is irrigation, which at 35.16%, would cover more than one-third of the area. In terms of distribution, this is mainly seen in the lower river area, and on the edge of the ridge. The latter is a reflection of the expected situation. Though, the total amount of irrigated areas is sincerely overestimated compared to the ground situation. This also seems to be the case with the land class houses. There are also some larger urban areas classified throughout the area, which not correspond to the real situation. The quantity and location of dark evergreen vegetation seems similar to the situation on the ground, like the classes non irrigated fields and light seasonal vegetation.

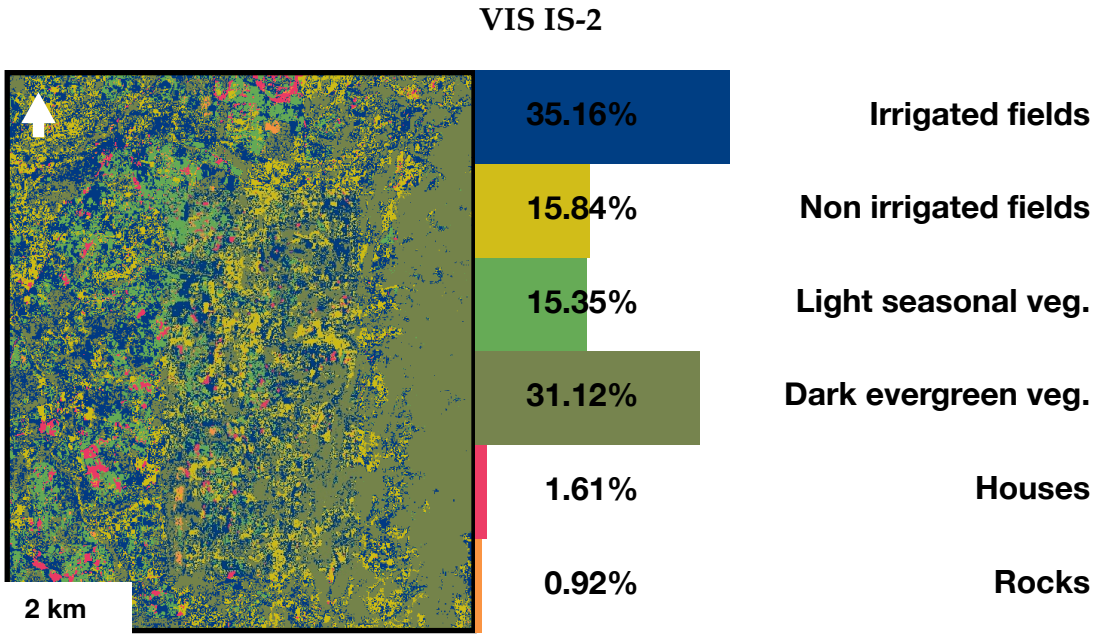

Figure 4.4.4. Classification map showing estimated land use for the visual (VIS: 2,3,4,8) band combination in irrigation season 2 (17/08/2017 to 20/11/2017).

4.4.5. IR IS-2

This prediction seems to show similar outcomes as that of VIS IS-2 in terms of dominant land classes and their distribution. However, this classification shows far fewer urban areas and more rocky areas, which also not correspond to the situation on the ground.

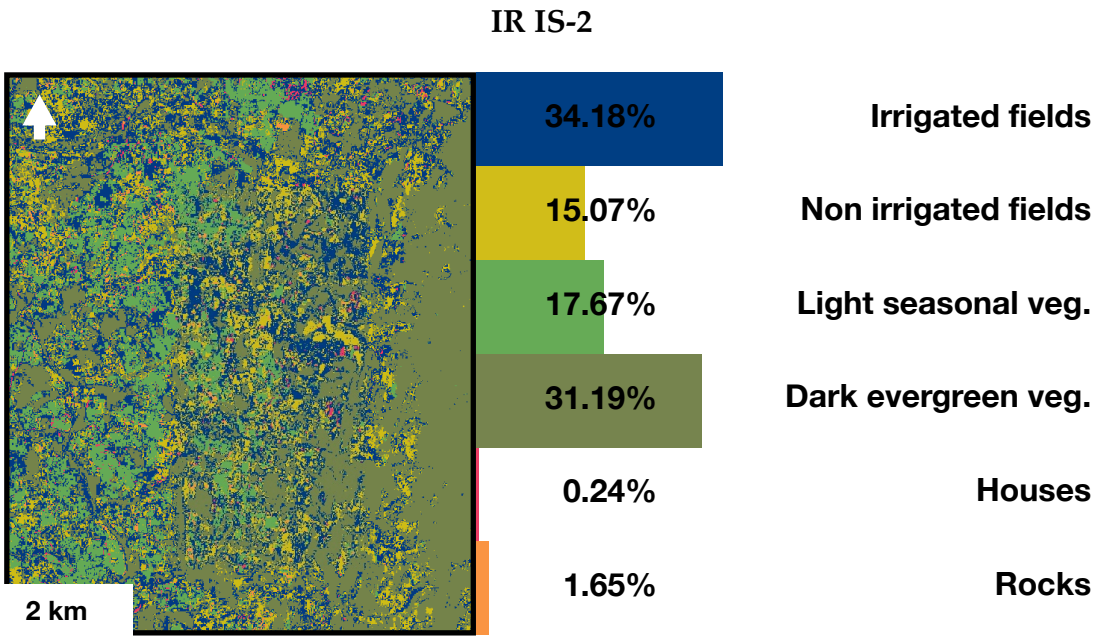

Figure 4.4.5. Classification map showing estimated land use for the infrared (IR: 4,8,11,12 band combination in irrigation season 2 (17/08/2017 to 20/11/2017).

4.4.6. RE IS-2

This classification also sincerly overestimates the amount of irrigated areas, as well as the land covers houses and rocks. The map shows that part of the large bushy are on the ridge is also classified as light vegetation, which actually reflects the real situation.

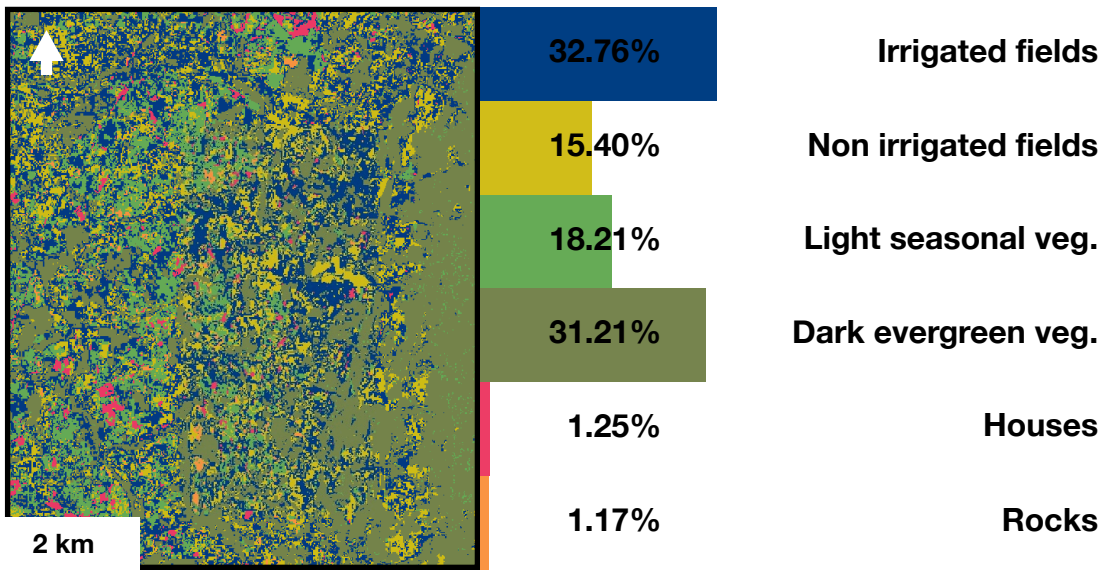

Figure 4.4.6. Classification map showing estimated land use for the red-edge (RE: 4,5,6,7,8,8A,11,12) band combination in irrigation season 2 (17/08/2017 to 20/11/2017).

In conclusion, the different classification maps show inconsistent resuls. The first irrigation season shows a big difference between the predictions of de VIS band combination and those of IR and RE. For irrigated fields, it predicts 23.37%, to 17.03% and 16.19% respectively. For non irrigated fields, 28.42%, relative to 38.03% and 37.77% for the IR and RE bands, and for light seaonal vegetation, 12.64% to 7.82% and 6.06%. The situations that seem to be most similar in terms of ground truth are those of the IR and RE band combinations. All band combinations in the second irrigation season predict about equal percentages of the different land classes, although the percentage of irrigated areas is about 3 times the expected value for all these classifications.

4.5. Accuracy assessment

To understand the underlying processes leading to the creation op these maps, and to evaluate the performance of the classification algorithm, accuracy assessment is performed. This is done for the classification with the highest κ accuracies achieved. Namely, for the red-edge band combination in both irrigation seasons using a random forest algorithm with 100 trees. The producers, users and overall accuracy of the training matrix from IS-1 using a 80% training split is depicted in table 4.5.1., and the validation matrix for the same classification in table 4.5.2. The same figures based on information from the second season are shown in figure 4.5.3. and the validation matrix in fiugure 4.5.4. The complete training matrices are in Appendix C.

4.5.1. Training matrix irrigation season 1

A score of nearly a 100% OA on the training matrix leaves little margin for confusion between the different classes. The only class that achieves 100% on both the PA and CA is rocks, this is also the class that consists of the fewest polygons (5). The PA of LSV is 93.3% and means that this class is often excluded, when it should not be.

Training PA, CU and OA of irrigation season 1 red-edge

	IF	NIF	LSV	DEV	H	R	OA%
PA%	99.4	97.6	93.3	99.7	98.1	100	98.2
UA%	97.7	96.9	98.8	99.9	100	100	

Table 4.5.1. Training accuracy of RF (100) based on RE bands, from irrigation seaon 1, κ is 97.6%.

4.5.2. Testing matrix irrigation season 1

The PA of houses of 50.9% is one of the most noticeable values of the testing matrix from the first irrigation season. This shows that this class is often not classified as being houses, when in fact it should be. The light seasonal vegetation class is often misclassified as both irrigated and non irrigated fields. In addition, the PA of non irrigated fields is 7% higher than its CA and this means that it is more often not included in the classification than it is. A large difference between PA (80.6%) and CA (100%) can also be found in the land class rocks, but the small size of this class makes it sensitive to change, and therefore sensitive to chance.

Testing matrix irrigation season 1 red-edge bands

	IF	NIF	LSV	DV	H	R	PA%
IF	392	36	7	4	1	0	85.3
NIF	38	334	13	4	0	0	87.4
LSV	11	17	116	4	0	0	84.5
DEV	4	2	1	244	0	0	95.9
H	6	3	2	0	33	0	50.9
R	1	1	0	0	0	18	80.6
UA%	87.2	80.4	83.5	94.8	97.9	100	88.0

Table 4.5.2. Testing accuracy of RF (100) based on RE bands, from irrigation seaon 1, κ is 81.7%.

4.5.3. Training matrix irrigation season 2

As with the training PA, CU and OA of irrigation season 1, an overall accuracy of 98.1% leaves little margin for confusion between the different classes. Again, most confusion arises in the light seasonal vegetation class, with a PA of 93.3%.

Training PA, CU and OA of irrigation season 2 red-edge

	IF	NIF	LSV	DEV	H	R	OA%
PA%	99.5	97.1	93.3	99.8	98.6	100	98.1
UA%	97.7	97.3	98.1	99.9	100	100	

Table 4.5.3. Training accuracy of RF (100) based on RE bands, from irrigation seaon 2, κ is 97.5%.

4.5.4. Testing matrix irrigation season 2

The testing matrix of IS-2 shows similarities with that of the first irrigation season. Here, a PA of 52.4% from the class houses, is eminently the lowest score. Here, the class dense vegetation is often underclassified, due to a higher PA than CU, of 5,6%.

Testing matrix irrigation season 2 red-edge bands

	IF	NIF	LSV	DEV	H	R	PA%
IF	351	31	2	10	3	0	86.2
NIF	26	346	10	5	1	0	84.1
LSV	13	16	109	2	0	0	81.4
DEV	8	2	2	239	0	0	95.3
H	7	3	1	1	32	0	52.4
R	2	0	0	0	1	21	95.7
UA%	83.0	81.8	85.9	89.7	96.5	100	88.3

Table 4.5.2. Testing accuracy of RF (100) based on RE bands, from irrigation season 2, κ is 84.1%.

4.6. Spectral signatures

Although the overall accuracy assessment of the quantitative analysis gives promising results, qualitative evaluation of the maps show inconsistency of classifications. Spectral signatures of the different land classes are analyzed to understand the differences on which the classifier distinguishes. The results presented are limited to irrigated fields, non irrigated fields and light seasonal vegetation, because of the interest to this study and their similarities on both field and data level. The spectral signatures of these land classes are presented by band combination on which the classifications are based.

4.6.1.Visual bands B2, B3, B4, B8

In general, there are no noticeable differences between the signals of the four band combinations. The non-irrigated fields signal shows a smoother transition between

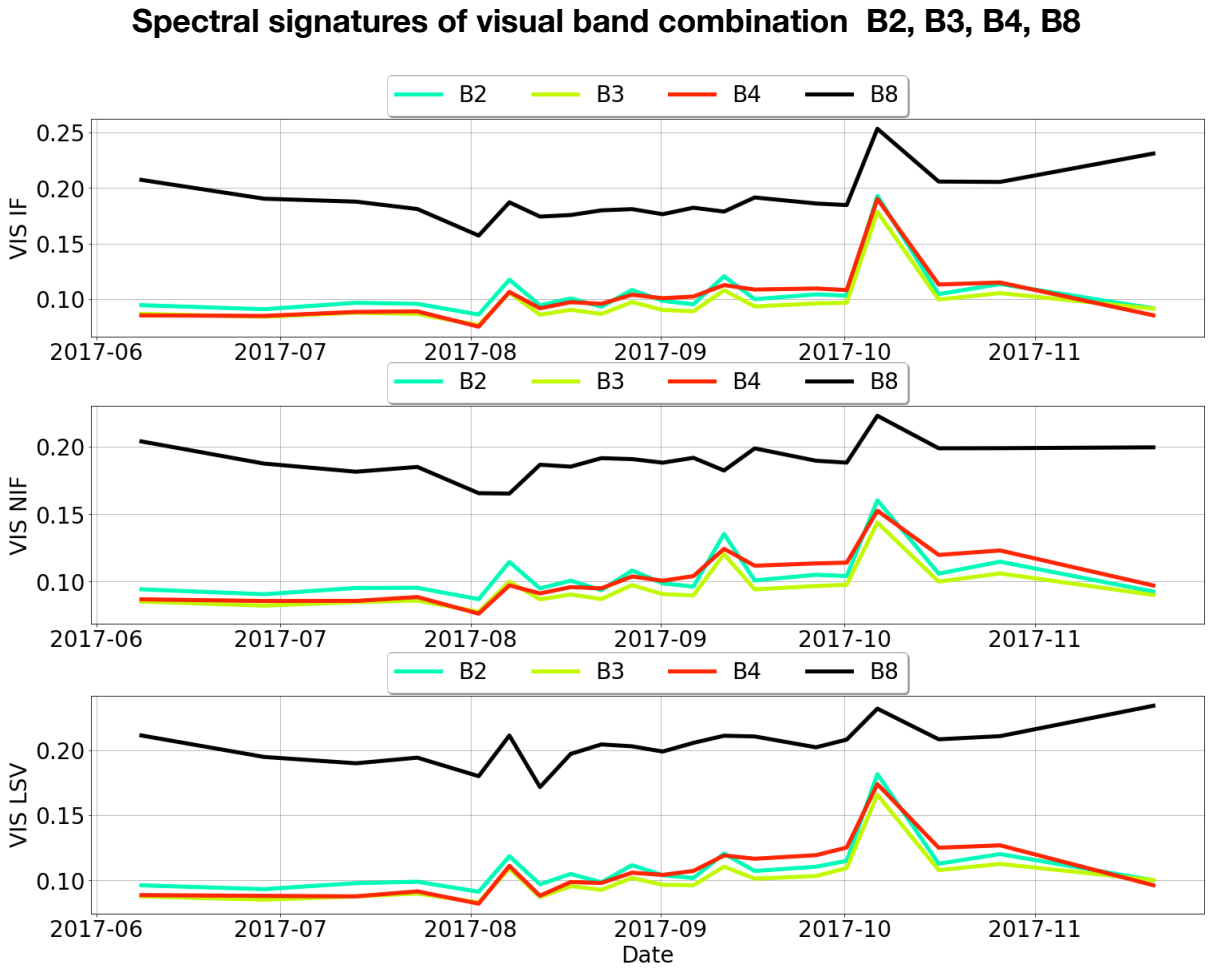

Figure 4.6.1. Mean spectral responses of the land classes irrigated fields (IF), non irrigated fields (NIF) and light seasonal vegetation (LSV), interacting with the visible (VIS: 2,3,4,8) bands. Data is based on Sentinel-2 images from 08/06/2017 to 20/11/2017 with a cloud threshold of 20%.

IS-1 and IS-2. After October, the B8 signal of this land class decreases, while that of the other land classes for this signal increases.

4.6.2. Infrared B4, B8, B11, B12

With this collection of spectral bands, some differences are detectable in the signal of B11 and B12. The light seasonal vegetation B11 and B12 shows a more gradual course in the second irrigation season.

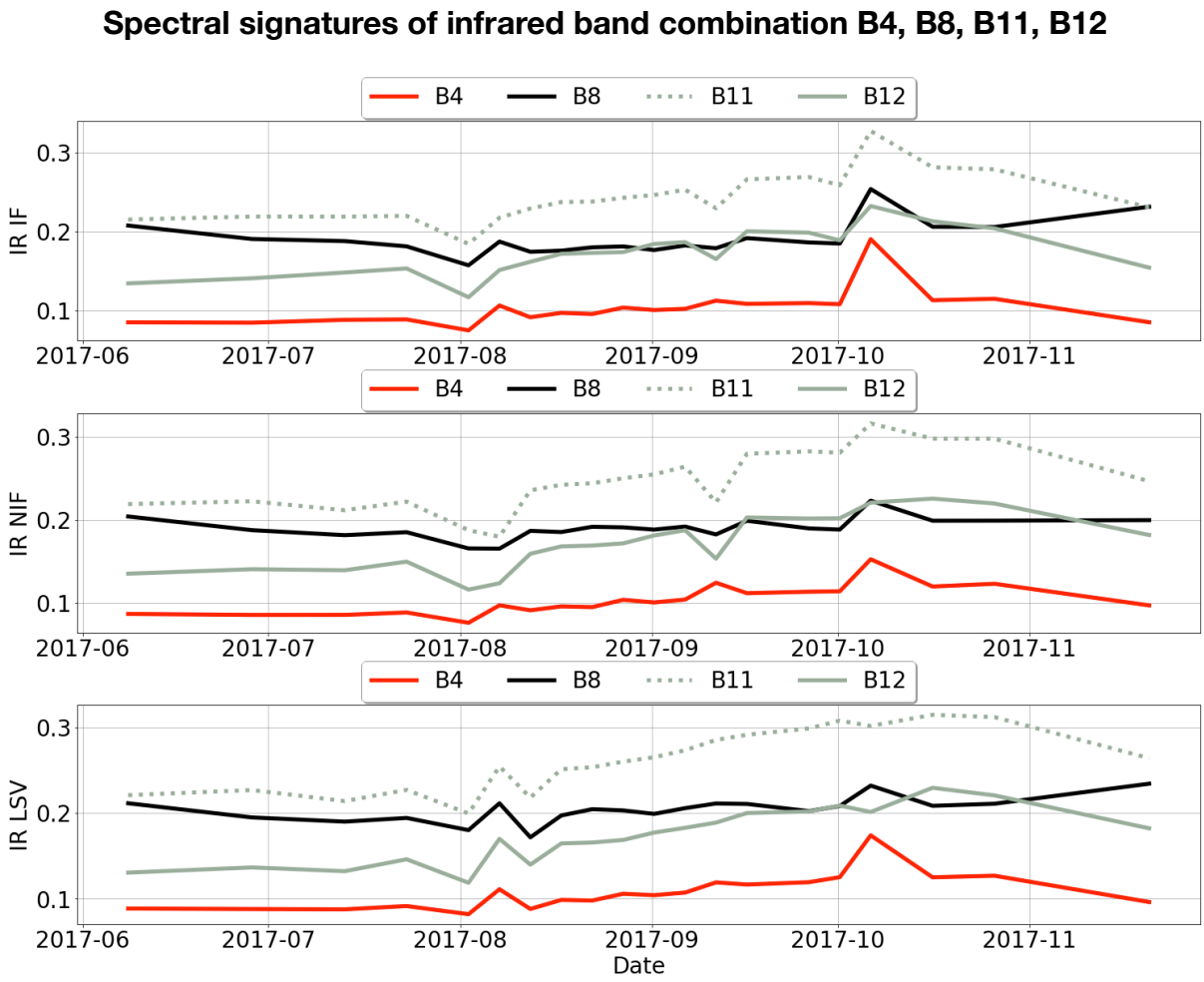

Figure 4.6.2. Mean spectral responses of the land classes irrigated fields (IF), non irrigated fields (NIF) and light seasonal vegetation (LSV), interacting with the infrared (IR: 4,8,11,12) bands. Data is based on Sentinel-2 images from 08/06/2017 to 20/11/2017 with a cloud threshold of 20%.

4.6.3. Red-edge B4, B5, B6, B7, B8, B8A, B11, B12

B5, B6 and B7 are also included in this band combination. These combinations are also not able to provide insight into spectral differences on which the classifier could distinguish.

The figures show are very low variability between the different land uses, as expected. As a result, it cannot be understood what spectral distinctions the classifier sees, in order to perform the classification. Only a small difference can be seen on B8, B11 and B12 and that could explain the highest accuries achieved with a classification based on red-edge bands. However, these results are too insignificant to make an informed statement on this.

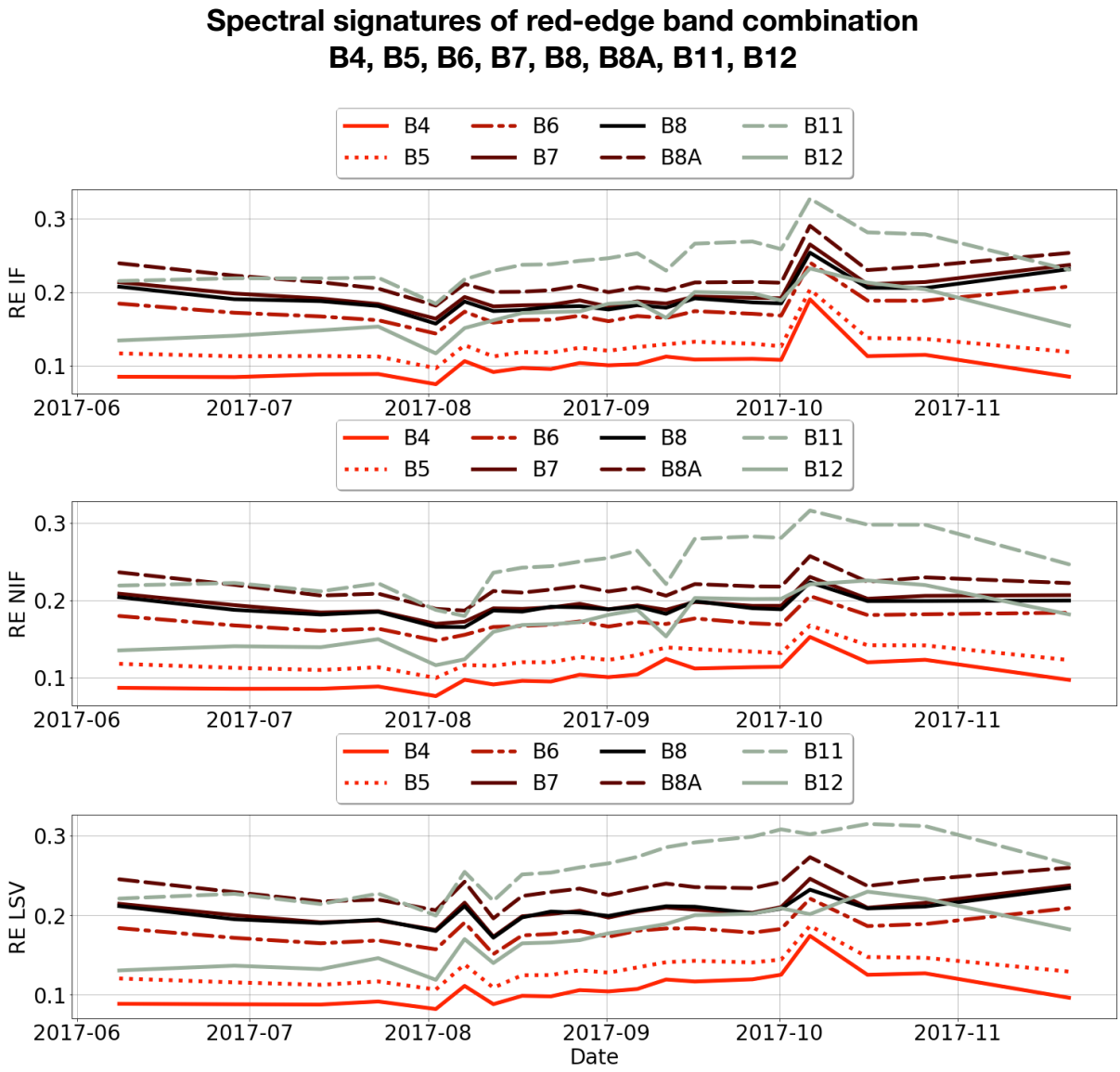

Figure 4.6.3. Mean spectral responses of the land classes irrigated fields (IF), non irrigated fields (NIF) and light seasonal vegetation (LSV), interacting with the red-edge (RE: 4,5,6,7,8,8A,11,12) bands. Data is based on Sentinel-2 images from 08/06/2017 to 20/11/2017 with a cloud threshold of 20%.

4.7. Potential of SAR Sentinel-1 data

This study attempts to reduce the problem of low inter-class spectral separability as indicated before by using ingenious non-parametric machine learning techniques for classification. The problem is caused in particular by the similarity between irrigated fields and light seasonal vegetation on field scale. It is examined whether S-1 SAR data is able to provide additional insight into the temporal behavior of these, and other land uses.

4.7.1. Intra class variability

The mean and standard deviations of the VV and VH backscatter intensities are depicted in figure 4.7.1., 4.7.2. and 4.7.3. The figures are construced using median aggregation, to account for the apparent effect of outliers of the logarithmically scaled dataset. When all figures are considered together, it can be seen that the variation within the dataset is greater than the variation between the different classes. The standard deviations become larger as the two irrigation seasons begin, for all classes and both polarizations.

Irrigated fields

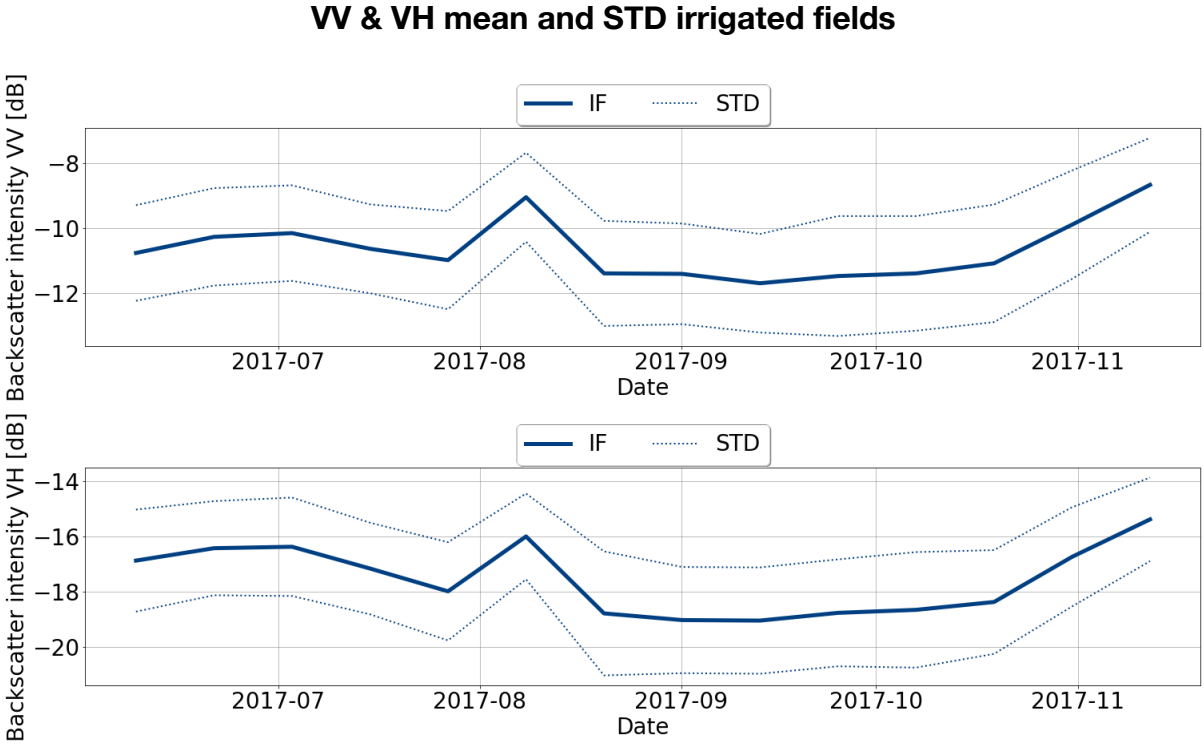

Figure 4.7.1. Temporal behavior of the VV and VH polarizations with the class irrigated fields (IF), expressed as the mean and standard deviation (STD) of the median aggregated Sentinel-1 dataset, images from 08/06/2017 to 20/11/2017

The mean of the first irrigation season of the VV signal is around -10.5 dB, and around -11.5 dB in the IS-2. For the VH signal, it is about -17 dB in IS-1, and -19 dB in IS-2. Both signals decrease again at the end of the second season, and show similarities in their course in general.

Non irrigated fields

In the first irrigation season, the mean of the VV signal is around -11 dB, and -12.5 dB in IS-2. For the VH signal, it is about -16 dB in the first half of IS-1, and -17 dB in the second half of IS-1. In irrigation season 2, the signal is about -17 dB.

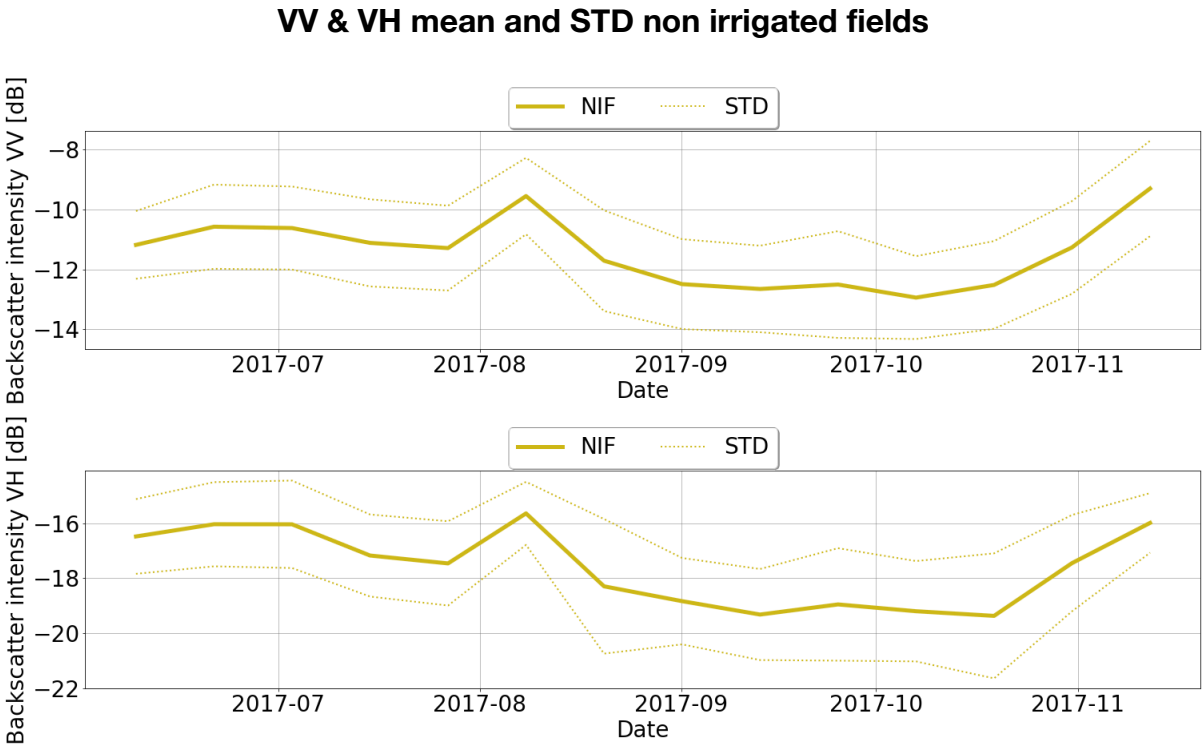

Figure 4.7.2. Temporal behavior of the VV and VH polarizations with the class non irrigated fields (NIF), expressed as the mean and standard deviation (STD) of the median aggregated Sentinel-1 dataset, images from 08/06/2017 to 20/11/2017

Light seasonal vegetation

For this land class, the mean of the first irrigation season of the VV signal is around -12 dB, and -13 dB in the IS-2. For the VH signal, it is about -17 dB in the first half of IS-1, and -18 dB in the second half of IS-1. In irrigation season 2 , the signal shows almost -20 dB.

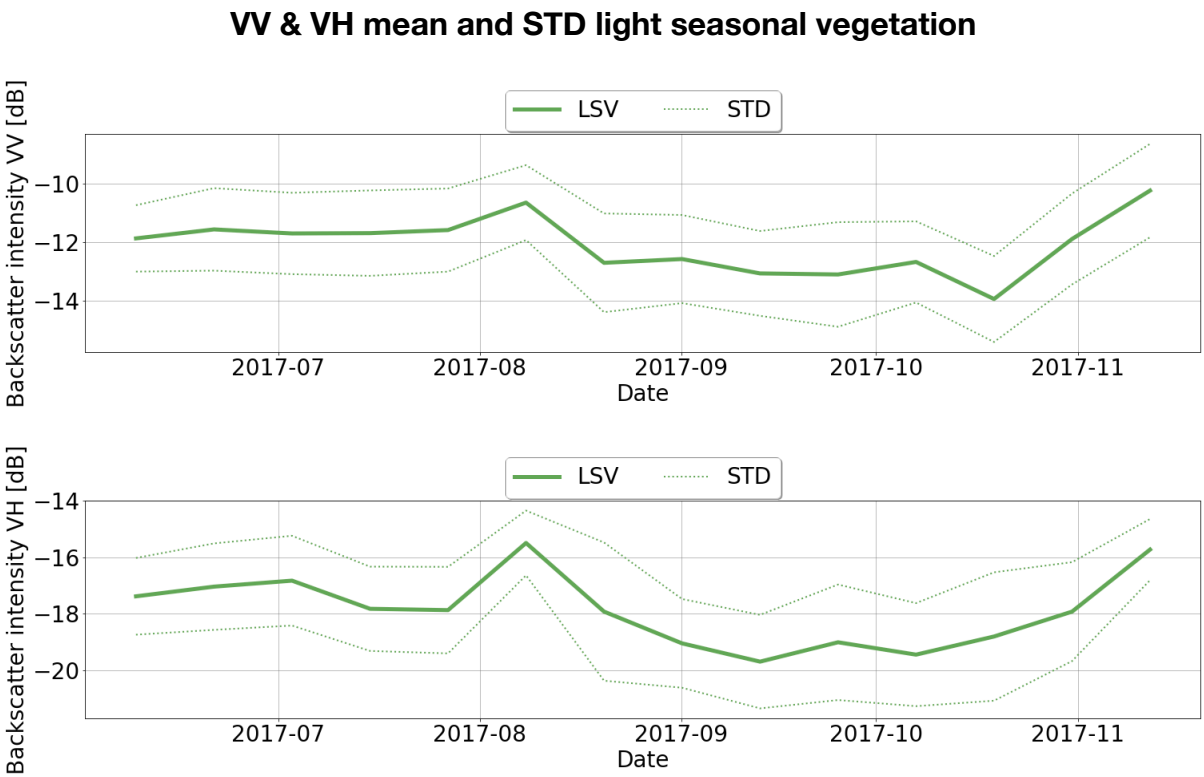

Figure 4.7.3. Temporal behavior of the VV and VH polarizations with the class light seasonal vegetation (LSV), expressed as the mean and standard deviation (STD) of the median aggregated Sentinel-1 dataset, images from 08/06/2017 to 20/11/2017

4.7.2. Inter class variability

Figure 4.7.4. shows the mean backscatter intensities in decibel of the VV and VH polarizations signal interacting with the classes irrigated fields, non irrigated fields and light seasonal vegetation, derived from all available information from the year 2017. This is to understand patterns on which the classifier could perform the classification.

The VV irrigation and non irrigation lines follow a similar pattern until September, as the second irrigation season begins. The light seasonal vegetation signal deviates from the two others earlier in the year, and begins to increase as of June. This signal continues to differ from that of IF and NIF until August, where the signals all converge and peak, showing a decrease in backscatter intensity at this time.

From the second irrigation season onwards, the VV polarizations of the different land classes diverge even further than in the first. During this period, the non irrigation signal is also approaching the signal of light seasonal vegetation. The NIF

and LSV signal overlap a few times a year. The VV signal of irrigated fields, with the exception of early April, always remains above that of the others two classes.

All VH polarization signals follow a similar pattern to that of VV, only the difference between the signals is smaller. A final notable difference from the VV is that, the non- irrigation signal is above that of irrigation in the first irrigation season, while in the second irrigation season it is reversed.

The most distinctive period for separating the signals irrigated fields and light seasonal vegetation is with the VV polarization in the second irrigation season.

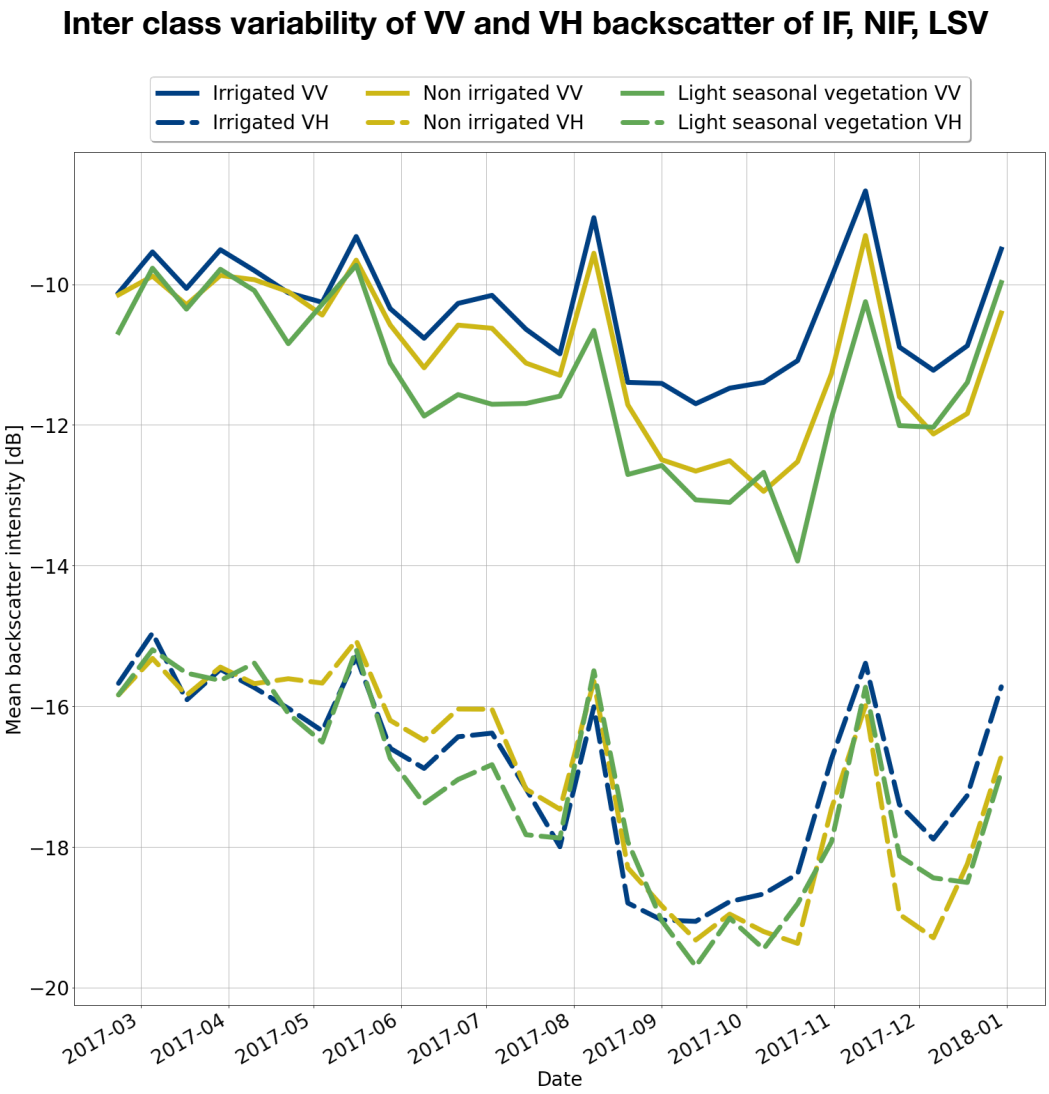

Figure 4.7.4. Temporal behavior of the VV and VH polarizations with the classes irrigated fields (IF), non irrigated fields (NIF) and light seasonal vegetation(LSV) expressed as the mean of the median aggregated Sentinel-1 dataset, images from all available information from 2017.

4.8. Accuracy assessment

Signal analysis shows that the problem of inter-class spectral separability of irrigated fields and light seasonal vegetation can best be overcome by using information from the VV polarization in irrigation season 2. How the model classifies based on this information can be evaluated by table 4.8.1. and table 4.8.2., the training and testing matrix of this classification, and the classification map shown in figure 4.8.3.

4.8.1. Training matrix

An overall accuracy of 94.5% is mainly caused by confusion between several classes. The lowest score consists of that of a PA of 88.7% in the light vegetation class, while its UA is 7% higher. The irrigated field class shows an inverse pattern, its PA is 5% higher than its UA. Pixels in this class are included in the classification, while those of light seasonal vegetation often should have been included. The pixels of these classes are most often confused with those of non irrigated fields.

Training matrix 08/06 -11/21 Sentinel-1 VV

	IF	NIF	LSV	DEV	H	R	PA%
IF	1638	34	3	10	0	0	97.2
NIF	84	1469	12	5	0	3	93.4
LSV	13	50	536	3	0	2	88.7
DEV	37	14	5	1062	1	0	94.9
H	4	4	3	3	185	0	92.9
R	1	1	1	0	0	105	97.2
UA%	92.2	93.4	95.7	98.1	99.5	95.5	94.5

Table 4.8.1. Training accuracy matrix of random forest classification with 100 trees based on VV polarizations from IS-2. The κ of the training set is 92.6%.

4.8.2. Testing matrix

With an overall accuracy of 64.6%, this testing matrix scores almost 30% lower than its training matrix. In particular, the class houses causes much confusion, with a UA of 44.9% and a PA of 36.1%. Furthermore, the UA of the light seasonal vegetation class is with 68.3% much higher than its PA of 55.2%. This means, that it is often incorrectly included in the classification. The light seasonal vegetation class is often confused with non irrigated fields, this also applies to the irrigated fields class. It is also most often confused with non irrigated fields. However, this method seems to be capable to some extent of distinguishing these classes from each other. But in general, the outcomes of the testing matrix are inconsistent and the PA and UA scores are too low, in order to be able to peform a reliable classification.

Testing matrix 08/06 -11/21

	IF	NIF	LSV	DEV	H	R	PA%
IF	302	62	14	55	10	1	68.0
NIF	80	263	18	12	9	10	67.1
LSV	21	40	95	11	3	2	55.2
DEV	56	22	3	182	5	1	67.7
H	10	18	6	5	22	0	36.1
R	1	2	3	2	0	15	65.2
UA%	64.3	64.6	68.3	68.2	44.9	51.7	64.6

Table 4.8.2. Testing accuracy matrix of random forest classification with 100 trees based on VV polarizations, from IS-2. The κ of the testing set is 52.6%.

Classification map

The inconsistent results of the confusion matrices are also qualitatively shown on the classification map in figure 4.8.3.The results are fragmented and do not reflect the ground situation by any means. All land classes are intermingled and do not show characteristic landscape patterns. On the right side of the ridge, according to this classification, many rocks occur, while this part mainly consists of dense evergreen vegetation.

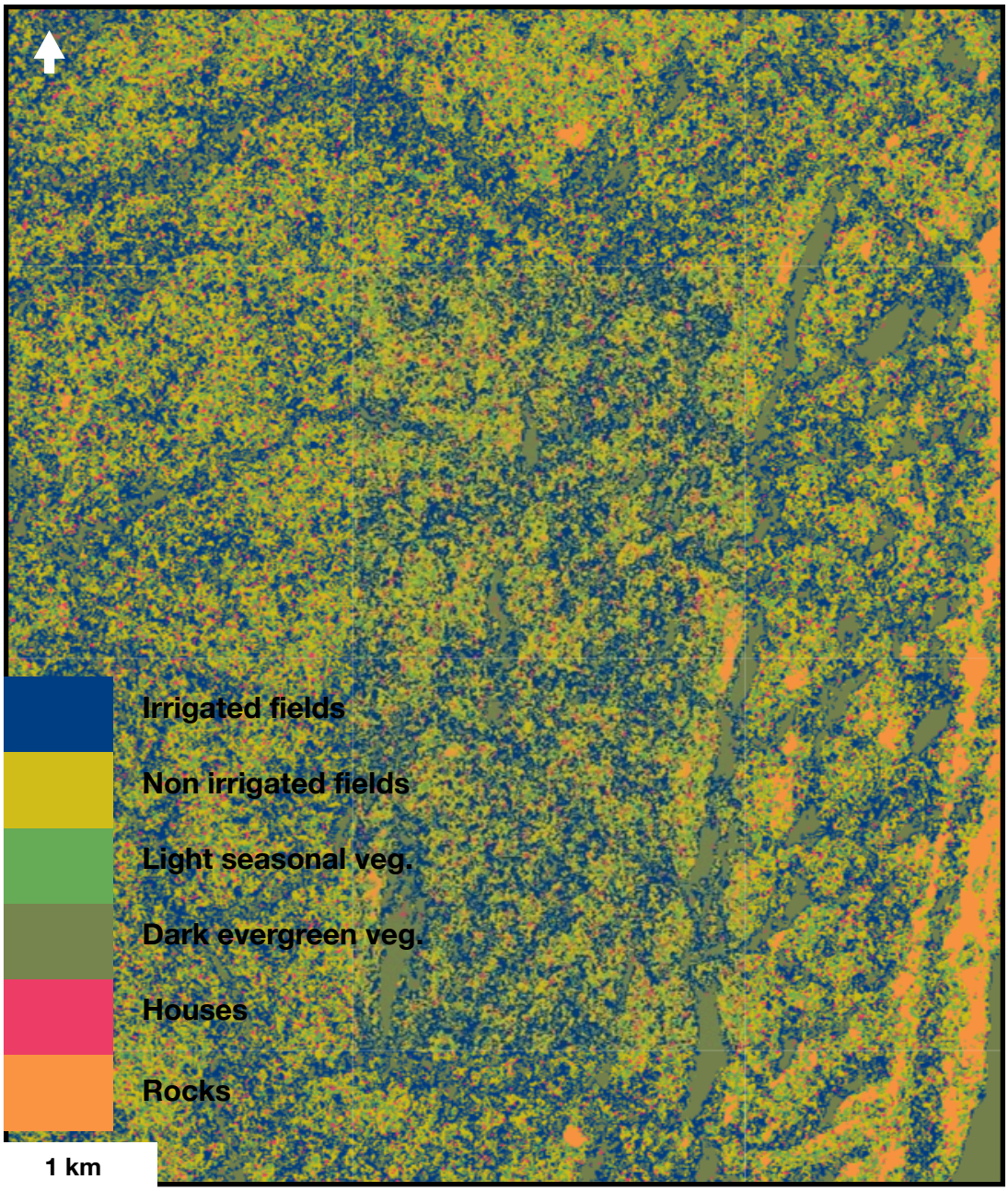

Figure 4.8.3. Classification map showing estimated land uses of a random forest classification with 100 trees based on VV polarizations from IS-2.

4.8.4. Accuracies of different training data sets

Both the quantitative and qualitative analyses show inconsistent results. From the hypotheses proposed and the results generated, a number of factors were identified that most likely contribute to this inconsistency. These are:

- The confusion which causes the class houses, as can be seen in the confusion matrix.
- The confusion which causes the class rocks, as can mainly be seen in the classification map.
- The relative large amount of polygons from the class irrigated fields, relative to the other land classes.
- The small size of the polygons of the class irrigated fields, compared to the size of the polygons of other land classes, as can be seen in Appendix A.
- The confusion in identification that might be caused by irrigated fields, which are adjacent to non irrigated fields.

To examine if these parameters have some effect on the classification, table 4.8.4. is created showing the PA and CA of six different classifications, and their training and testing κ accuracies. These classifications are all done based on a random forest classification with 100 trees with imagery from 09/01/2017 to 11/24/2017, using the following subsets of training data, consisting of:

- All polygons from all classes, using VV polarization mode.
- All polygons from all classes, using VH polarization mode.
- All polygons from all classes, using VV and VH polarization mode.
- Polygons from irrigated fields, non irrigated fields, light seasonal vegetation and dark seasonal vegetation, using VV polarization mode.
- The 42 out of 146 largest polygons of irrigated fields, using VV polarization mode.
- The 42 out of 146 largest polygons of irrigated fields, light seasonal vegetation, dark evergreen vegetation, houses and rocks using VV polarization mode.

The only subset that scored higher than the examined one is the one using large irrigated fields and without non irrigated fields, which reaches an accuracy of 67.1%.

Accuracies of different training sets

Classes		IF	NIF	LSV	DEV	H	R	κ	
IF - NIF - LSV - DEV - H- R	**VV**	64.1	64.9	50.6	68.1	33.1	55.2	64.1	**PA%**
		64.7	63.4	52.6	72.1	44.4	72.2	51.9	**CA%**
IF - NIF - LSV - DEV - H- R	**VH**	63.2	76.4	48.4	76.1	32.4	48.3	63.4	**PA%**
		61.9	64.8	52.4	71.6	52.2	53.8	51.1	**CA%**
IF - NIF - LSV - DEV - H- R	**VV VH**	69.9	60.5	39.5	70.2	15.8	56.3	60.9	**PA%**
		62.8	55.7	52.4	70.2	37.5	72.0	47.5	**CA%**
IF - NIF - LSV - DEV	**VV**	69.1	64.1	56.3	71.4			60.5	**PA%**
		66.2	67.6	60.2	68.5			52.9	**CA%**
LARGE IF - NIF - LSV - DEV - H- –	**VV**	63.1	64.5	51.0	71.6	27.5	56.3	62.4	**PA%**
		56.8	64.9	52.0	76.4	28.8	56.3	50.4	**CA%**
LARGE IF - LSV - DEV - H- R	**VV**	69.3		65.0	74.4	34.5	48.3	67.1	**PA%**
		69.3		62.2	73.6	40.4	56.0	53.9	**CA%**

Table 4.8.4. Accuracies of different test data sets, from images with dates: 09/01, 09/13, 09/25, 10/07, 10/19, 10/31, 11/12, 11/24. Constructed of median reduced SAR data with an incidence angle of 40.1 degrees. Based on a RF (100) classifier and a split of 80/20 in training and testing data. The large irrigated field class consists of the 42 out of 146 largest polygons.

5. Discussion

The discussion consists of two parts. Section 5.1. reviews the broader context of this research. Section 5.2. discusses several assumptions and decisions that were made during the research, and might affect the results obtained.

5.1. Using S-1 and S-2 data to map farmer-led irrigated agriculture

This research aims to provide insight into the usefulness of remotely sensed passive Sentinel-2 Level-1C and active Sentinel-1 SAR data for automatic detection of farmer-led irrigated agriculture in Central Mozambique. For this purpose, an open source-code is written, in the form of a model, that uses open-source satellite data from Google Earth Engine to execute the methodology developed. Research in the specific case study area contributes to developing a tool for identifying smallholder irrigation using satellite data, that can be scaled to the required national level. In addition, it contributes to the fundamental research on supervised image classification of complex agricultural landscapes, with optical and radar remotely sensed data and machine learning.

What is the performance of the new model, compared to the old method (Hollander, 2018)

The main classification challenge in this area is working with training data that has a high degree of intra variability and in which there is little variability between the land classes, not at all those of irrigated fields and light seasonal vegetation. The results of this research seem to confirm the hypothesis that a nonparametric classifier is more suitable to handle the highly variable data than a parametric one, since it does not assume that the statistics of the land classes are normally distributed. The nonparametric random forest classifier provides a little higher κ accuracy (88.0%) than the parametric maximum likelihood classifier (85.0%) as used by Hollander (2018), where both κ's are based on classifications with Sentinel-2's Red-Edge and SWIR bands: 4,5,6,7,8,8A,11,12 using images from irrigation season 2.

What is the potential of Sentinel-2 data using a Random Forest classifier to identify smallholder irrigation in Manica, Mozambique?

Random forest classifications, constructing 100 trees with information from RE band combinations, reach OA's of (88.0%) in IS-1 and (88.3%) in IS-2. According to this chosen accuracy assessment method using a confusion matrix, this would quantitatively mean that the classification was reasonably successful. However, classification maps do not show realistic outcomes in terms of quantity of predicted land covers and their distribution throughout the area. The estimated irrigated area based on classifications with RE bands is 16% and 33%, in IS-1 and IS-2 respectively and therefore lower than the predicted area based on VIS (23% and 35%) and IR (17% and 34%) bands. However, it was identified by Hollander (2018) that approximately 10-15% of the total area was irrigated, and all classifications with the RF classifier overestimate this amount significantly.

To gain insight into the underlying mechanisms of the classification algorithm, spectral analysis of the various bandwidths is performed. The temporal spectral signatures of the land classes show low variability between classes and high variability in terms of standard deviation within the classes, which provides no further information. The κ accuracies of the classifications based on chlorophyll sensitive Red Edge and SWIR bands provide the highest values: 0.77% for the IR and 0.87% for the RE band combination, in IS-1. These values are respectively 0.74% and 0.88% in the second irrigation season. Both classifications make us of bands B4, B8, B11, B12 and the RE band combination additionally uses B5, B6, B7 and B8A .

Therefore, it could be that irrigated agriculture with Sentinel-2 data can be identified on the basis of an increase in vegetation biomass or that the classifier benefits from more information through the use of multiple bands. Yet, this is not reflected in the spectral response behavior and as a consequence, it is unclear on the basis of which spectral distinction the model seperates the data, which lead to these results.

What is the potential of Sentinel-1 data using a Random Forest classifier to identify smallholder irrigation in Manica, Mozambique?

Research on Sentinel-1's potential do seem to provide differences in response behavior of the backscatter intensities, when considering the mean behavior of the polygons of the land classes irrigated fields, non irrigated fields and light seasonal vegetation. Time series of the VV backscatter intensities do show a signal difference

between the irrigation class and the classes non irrigated and light seasonal vegetation in irrigation season two. However, high standard deviations do reflect the high intra variability of the data, and classification accuracies in this period do not exceed an overall accuracy of 64.1%. The main confusion as identified by the confusion matrices, comes from classes that are often identified as irrigation, whereas they are not, overestimating the amount of irrigated areas as with the use of S-2 data. When testing with different data subsets, only the tests that used the 25% largest polygons of irrigated fields yield a higher OA of 67.7%. However, this difference is too insignificant to explain the cause of confusion and does not offer further insight into the model's decision processes.

5.2. Reflection of results

This research appears to show that the used method and data collections do not provide accurate information for the intended classification goal. However, the research method is based on several assumptions that influence the classification outcomes. In this section, these assumptions are critically discussed and compared to literature.

5.2.1. Sentinel-1 & Sentinel-2 data for image classification in complex landscapes

The main debatabale issue of this research is whether the phenomenon being studied is spatio-temporal compatible with the context in which it is being studied.

Many studies have highlighted this issue on the complexity of using remote sensing for mapping parcel-level agricultural practices of smallholder farmers (Onojeghuo et al., 2018; Alganci et al., 2013). This complexity lies mainly in the small area of the croplands, with heterogenous cultivation and irrigation practices due to decentralized management (Lebourgeois et al., 2017; Piiroinen et al., 2015). These factors can greatly influence the variability of spectral signatures, which makes it difficult to assign specific characteristics to certain land classes (Onojeghuo et al., 2018). In addition, the size of a normal cropland in these complex agricultural landscapes is often greater than or the same as the pixel size of coarse-resolution satellite data, and therefore prone to misclassification (Wu et al., 2017).

Although this study uses medium-resolution satellite data (10-20 m), the intended classification object is often only a few pixels in size. This allows the classifier to obtain only a few pixels of class specific information from a single polygon. This increases the likelihood of both high variability of information and confusion with

surrounding classes, which makes the construction of a comprehensive knowledge base more unreliable, given the spatial scale on which this research is conducted.

The temporal variation of spectral signatures on which the classifications are based, complicate the classification process as well. Figures 4.6.1., 4.6.2. and 4.6.3. show variable and inconsistent signatures, which makes it difficult to assign specific characteristics to a certain land class.

5.2.2. Pre-processing

Cloud filter of Sentinel-2 data

Sentinel-2 data as used in the previous study uses Top-of-Atmospere data that is converted to Bottom-of-Atmosphere images with Sen2Cor (Hollander, 2018; SNAP, 2018; Müller-Wilm, 2016). This research makes use of Sentinel-2 Level-1C orthorectified top-of-atmosphere reflectance data. The TOA product has proven its reliability on image classification from various studies, since relative spectral differences are the key aspect (Song et al., 2001).

This however, in combination with the cloud filter and cloud mask used could explain the differences in overall κ accuracies of the classifications achieved (table 4.2.1), compared to those of the maximum likelihood classifier as used in the previous research (Hollander, 2018). The κ accuracies of Hollander (2018) do not show corresponding outcomes with the support vector machine, classification and regression trees and random forest classifiers as used in this research. There is no pattern to be seen, as well in irrigation season as in used band combinations.

Hollander (2018) makes use of cloud-free imagery, which results in less images available to the machine learning model in irrigation season 2 (7 instead of 13). Because mosaicing is used as aggregation method, spatially overlapping datasets are combined into a spatially continious image. This therefore results in more data available to the machine learning model in this research, from which more information can be extracted to assign specific characteristics to a land class.

Speckle filter of Sentinel-1

One of the difficulties in handling SAR data is the presence of speckle effects, which is caused by the interference of backscatter between adjacent retrievels (Goodman, 1976). This speckle effect provides a random granular texture on images, making

visual interpretation challenging. S-1 data retreived from GEE is multi-look processed, for the purpose of correcting standard noise and reducing the effect of speckle (Jin et al., 2019).

Since this study uses GEE multi-look processed S-1 data, it was therefore decided not to apply an additional speckle filter. This might explain the following result, also noted by Jin et al. (2019): large-scale distinguishable features can by seen on images that are affected by speckle-noise; they can be severely compromised on a smaller scale. On figure 4.7.4., in the VV polarization signal there seems to be a difference in IS-2 between the different land classes irrigated fields, non irrigated fields and light seasonal vegetation when all polygons of a given class are viewed together. Classification accuracies in this period, however, do not exceed an overall accuracy of 64.1%, making the classification unreliable.

5.2.3. Use of data for classification

The supervised image classification method used requires the collection of training and validation data (Foody, 2004). Regardless of the used classifier, accuracy assessment is performed to determine the quality of the classification outcome, and various factors affect this accuracy assessment.

Quantity of reference data

When training and validation data is not obtained using a randomly distributed sampling strategy, the data can no longer be assumed to be independent. Which, according to several studies (Zhen et al., 2013; Friedl et al., 2000; Hammond et al.,1996), has led to optimistic bias towards classification and inflated accuracy outcomes (Hammond et al.,1996). In addition, machine learning algorithms may also be biased if the distribution of training and validation data is unequal or imbalanced relative to the actual situation on the ground. If so, the classification outcome may favour the main class in the training data (Breidenbach et al., 2010; He & Garcia, 2009; Foody & Mathur, 2004).

This research makes use of an opportunistic sampling method, in which as much information as possible was obtained from the land class irrigated fields, where the most interest is. As a result, there are about 10 times as many polygons of this land class (IF 146) than of, for instance, light seasonal vegetation (12). Furthermore, the OA of 88.0% seems optimistically biased, since qualitative assessement of the ground

situation does not show reliable classification outcomes. Additionally, the amount of irrigated agriculture is more than 3 times as much as expected in the area, making the model appear to be biased toward this most sampled land class.

Feature selection of the classifier

This study makes use of the random forest classifier that works as a black box model (Breiman, 2001). Since an ensemble of decision trees are built, it is not easy to illustrate how the predictions are made (Horning, 2010). To illustrate the selection process, all trees should be drawn and analyzed individually, and this was not done in this study. It is therefore unclear on the basis of which information the classifier categorizes the different land classes.

It is assumed that classification is based on differences in spectral and backscatter reponses when interacting with different land classes. However, in both the temporal signals of the spectral signatures (figures 4.6.1.; 4.6.2.; 4.6.3) and backscatter reponses (4.7.1.; 4.7.2.; 4.7.3) no clear difference can be demonstrated between the classes irrigated fields, non irrigated fields and light seasonal vegetation. Nonetheless, these figures show low variability between classes and high variability in terms of standard deviation within the classes.

Since the classification based on the chlorophyll sensitive Red Edge and SWIR bands, provides the highest overall accuracies, it appears that irrigated agriculture with Sentinel-2 data can best be distinguished on the basis of an increase in vegetation biomass. However, this study offers too little evidence to conclude this with certainty.

6. Conclusions & recommendations

This research aims to provide insight into the usefulness of remotely sensed passive Sentinel-2 Level-1C and active Sentinel-1 SAR data for automatic detection of farmer-led irrigated agriculture in Central Mozambique, using nonparametric machine learning techniques.

6.1. Conclusions

What is the potential of using Sentinel-1 and Sentinel-2 data to map farmer-led irrigated agriculture with machine learning? A case study in Central Mozambique

The results of this research show that the used method and data collections do not provide accurate information for the intended classification goal. Various factors contribute to this conclusion.

Classifications with the nonparametric random forest classifier provide a little higher κ accuracy (88.0%) than the parametric maximum likelihood classifier (85.0%) as used by Hollander (2018), where both κ's are based on information from S-2 RE bands in IS-2. Therefore, it appears that a nonparametric RF classifier is preferred over a parametric ML classifier for processing the data that is high in variability, since it does not assume a normal distribution of the statistics of the land classes.

However, the apparent improvement of κ accuracy is insignificant, and classification maps do not show realistic outcomes in terms of quantity and distribution of predicted land cover area. The estimated irrigated area is 16% in IS-1, and 33% in IS-2, based on RE bands where the overall accuracy is respectively 88.0% and 88.3%.

It was identified that ~ 10-15% of the total area is irrigated, and all classifications with the RF classifier overestimate this amount. This overestimation of irrigation is probably caused by the opportunistic sampling method, causing inflated accuracy outcomes and an optimistic bias towards classification of the main class in training.

Spectral analysis of the temporal behavior of various S-2 bandwidths does not provide insight into the underlying mechanisms on which the algorithm performs classification. The chlorophyll sensitive Red Edge and SWIR bands provide the highest κ accuracies in IS-1 and IS-2: 0.77% and 0.74% for the IR bands and 0.87% and 0.88% for the RE bands. Therefore, it appears that irrigated agriculture with S-2 data can be identified on the basis of an increase in vegetation biomass and that the classifier benefits from more information through the use of multiple bands. However, this research provides too little evidence to assume this with certainty.

Research into the use of Sentinel-1 SAR data appears to have potential for identifying irrigation when considering the temporal behavior of the mean backscatter intensities of different land uses. Time series of the VV signal show a difference between the irrigation class and the classes non irrigated and light seasonal vegetation in IS-2. However, high standard deviations do reflect the high intra variability of the data, and classification accuracies in this period, do not exceed an overall accuracy of 64.1%. The main confusion as identified by the confusion matrices, comes from classes that are often identified as irrigated, whereas they are not, overestimating the amount of irrigation as with the use of S-2 data.

In conclusion, random forest classification based on chlorophyll sensitive bands reach an OA of more than 88%, in both irrigation seasons. Based on the chosen accuracy assessment method, this classifier therefore seems to have sufficient potential for the classification product to be developed, which aims to identify irrigated agriculture at national level. However, the classifications are not reliable compared to the ground situation, overestimating the amount of irrigation by 3. This research demonstrates in several ways the complexity of supervised image classification of complex agricultural landscapes: the unbalanced and variable reference data, which often consist of only a few satellite pixels, make it difficult to identify characteristics of land classes, on which classification can be based. In which Sentinel-1 as added and used in this study, offers no additional insights.

6.2. Recommendations

Recommendations for identifying farmer-led irrigated agriculture in Central Mozambique are therefore given in 3 areas. 6.2.1. Discusses what has been researched to design the methodoloy in this study, and which for various reasons have been decided do not work. 6.2.2. Proposes a technique to improve the detection of irrigation in the specific case study area. 6.2.3. Suggests 2 ways of fundamental follow-up research on the field of using S-1 and S-2 data for classification of complex agricultural landscapes.

6.2.1. Development of the methodology

To design the methodology for this study, several things were attempted such as: Classification based on spectral indices such as the Normalized Difference Vegetation Index (NDVI) (Rouse et al., 1974), the Normalized Difference Water Index (NDWI) (Gao, 1996) and the Normalized Difference Infrared Index (NDII) (Hardisky et al., 1983) and co-polarization ratios (HH/VV) (Nguyen et al., 2016). Canny edge detection (Watkins & Van Niekerk, 2019), to delineate fields, change detection based on Sentinel-1 imagery (Canty et al., 2020; Canty, 2019; Conradsen et al., 2016; Conradsen et al., 2003), and hierarchical classification using both Sentinel-2 and Sentinel- 1 data such as in Mahdianpari et al. (2019). These methods have already been examined but proved to be ineffective with the reference and satellite data used, the model, or due to the complexity of the landscape, or did not produce better results than the method presented in this study. It is not recommended to investigate the aforementioned methods further in order to improve the classification of this specific case study area.

6.2.2. Citizen science

With all that has been tried, it can be concluded that from the signal of the collected training data no more can be obtained than has been achieved so far. Therefore, in order to improve the identification of farmer-led irrigated agriculture in Manica, other technologies for smart agriculture can be explored in addition to deploying satellite data, considering the complexity and variability of the landscape. Citizen science could engage the smallholder farmers to collect data on their irrigation and farming practices. This data can be used to gain large-scale insight into these practices, upon which water management can be adjusted. The wealth of information also allows to identify trends and challenges, which can be reported to individual farmers, allowing tailor made agricultural water management on field

level. This may include; an app that allows users to gather data on land use and land cover (Mourad et al., 2020), using SMS to provide farm related information (Beza et al., 2018) or combining citizen science and remote sensing for irrigation monitoring (Corbari et al., 2021).

6.2.3. Image classification for complex agricultural landscapes

Working with imbalanced data

The dataset used for this study is characterized by the high degree of variability. Collecting more or different data may reduce this variability somewhat, but it remains characteristic of these landscapes. Better consideration can therefore be given to advanced methods of performing image classification and accuracy assessement with imbalance datasets. The use of a weighted confusion matrix can be explored, that can provide more accurate accuracy assessment than using more traditional confusion matrices (Mellor et al., 2015). This research did not reveal on what information the classifier classifies, and therefore more research can be done on learning from imbalanced datasets (He & Garcia, 2009). This may provide more insight into the response of smallholder irrigation agriculture relative to other land classes, when these interact with different bands, indices, polarization modes and ratios of different satellite data, and thus into the underlying mechanisms of the algorithm. To better deal with the complexity of the landscape, it is also possible to look at spatial random forest algorithms that use spatial-spectral instead of pixelwise spectral information that also learn from intrinsic heterogeneity, spatial dependencies, and complex spatial patterns. These algorithms seem to be better at handling spatial dependencies and intrinstic heterogeneity which is characteristic of these complex agricultural landscapes (Talebi et al., 2021).

Speckle filters for small target areas

Investigating the use of a more complex speckle filter for using the multi-look processed Sentinel-1 GEE data product is strongly recommended. However, these speckle filters make use of a buffer zone, consisting of several pixels, like a $3x3$ pixel Boxcar filter or Lee of Refined Lee filter consisting of a $7x7$ pixel window (Foucher & López-Martínez, 2014). Since the intended target object in these landscapes is often only a few pixels in size, one can look at the amount and impact of the information loss when using such a filter. The main challenge with be to balance the need of speckle reduction and class specific information preservation.

7. Reflection

I would like to thank my main supervisor Martine Rutten, Timon Weitkamp from Resilience B.V. and the WUR, and my other supervisors Susan Steele-Dunne and Elisa Ragno for their help and support in my study, and their contribution to their own area of research. In addition, I just want to say thank you to my family, friends, roommates, colleagues and all the new people I have met in the past year. Although these are strange times, there was no better activity for me than getting a master's degree during a pandemic. You all made it a lot more fun and meaningful!

Floor Crispijn,
Delft, August 2021

Bibliography

Agurla, S., Gahir, S., Munemasa, S., Murata, Y., & Raghavendra, A. S. (2018). Mechanism of stomatal closure in plants exposed to drought and cold stress. *Survival strategies in extreme cold and desiccation*, 215-232.

Alganci, U., Sertel, E., Ozdogan, M., & Ormeci, C. (2013). Parcel-level identification of crop types using different classification algorithms and multi-resolution imagery in Southeastern Turkey. *Photogrammetric Engineering & Remote Sensing*, *79*(11), 1053-1065.

Ambika, A. K., Wardlow, B., & Mishra, V. (2016). Remotely sensed high resolution irrigated area mapping in India for 2000 to 2015. *Scientific data*, *3*(1), 1-14.

Balenzano, A., Mattia, F., Satalino, G., & Davidson, M. W. (2010). Dense temporal series of C-and L-band SAR data for soil moisture retrieval over agricultural crops. *IEEE Journal of Selected Topics in Applied Earth Observations and Remote Sensing*, *4*(2), 439-450

Bazzi, H., Baghdadi, N., Ienco, D., El Hajj, M., Zribi, M., Belhouchette, H., ... & Demarez, V. (2019). Mapping irrigated areas using Sentinel-1 time series in Catalonia, Spain. *Remote Sensing*, *11*(15), 1836.

Beekman, W., Veldwisch, G. J., & Bolding, A. (2014). Identifying the potential for irrigation development in Mozambique: Capitalizing on the drivers behind farmer-led irrigation expansion. *Physics and Chemistry of the Earth, Parts A/B/C*, *76*, 54-63.

Bégué, A., Arvor, D., Bellon, B., Betbeder, J., De Abelleyra, D., PD Ferraz, R., ... & R Verón, S. (2018). Remote sensing and cropping practices: A review. *Remote Sensing*, *10*(1), 99.

Beza, E., Reidsma, P., Poortvliet, P. M., Belay, M. M., Bijen, B. S., & Kooistra, L. (2018). Exploring farmers' intentions to adopt mobile Short Message Service (SMS) for citizen science in agriculture. *Computers and Electronics in Agriculture*, *151*, 295-310.

Blaschke, T., Hay, G. J., Kelly, M., Lang, S., Hofmann, P., Addink, E., ... & Tiede, D. (2014). Geographic object-based image analysis–towards a new paradigm. *ISPRS journal of photogrammetry and remote sensing*, *87*, 180-191.

Bousbih, S., Zribi, M., El Hajj, M., Baghdadi, N., Lili-Chabaane, Z., Gao, Q., & Fanise, P. (2018). Soil moisture and irrigation mapping in A semi-arid region, based on the synergetic use of Sentinel-1 and Sentinel-2 data. *Remote Sensing*, *10*(12), 1953.

Breidenbach, J., Næsset, E., Lien, V., Gobakken, T., & Solberg, S. (2010). Prediction of species specific forest inventory attributes using a nonparametric semi-individual tree crown approach based on fused airborne laser scanning and multispectral data. *Remote Sensing of Environment*, *114*(4), 911-924.

Breiman, L. (2001). Random forests. *Machine learning*, *45*(1), 5-32.

Burney, J. A., & Naylor, R. L. (2012). Smallholder irrigation as a poverty alleviation tool in sub-Saharan Africa. *World Development*, *40*(1), 110-123.

Bush, T. F., & Ulaby, F. T. (1978). An evaluation of radar as a crop classifier. *Remote Sensing of Environment*, *7*(1), 15-36.

Canty, M. J. (2019). Image Analysis, Classification, and Change Detection in Remote Sensing: With Algorithms for Python. Crc Press.

Canty, M. J., Nielsen, A. A., Conradsen, K., & Skriver, H. (2020). Statistical analysis of changes in Sentinel-1 time series on the Google Earth Engine. *Remote Sensing*, *12*(1), 46

Cawley, G. C., & Talbot, N. L. (2010). On over-fitting in model selection and subsequent selection bias in performance evaluation. *The Journal of Machine Learning Research*, *11*, 2079-2107.

Chakraborty, S., & Newton, A. C. (2011). Climate change, plant diseases and food security: an overview. *Plant Pathology*, *60*(1), 2-14.

Coluzzi, R., Imbrenda, V., Lanfredi, M., & Simoniello, T. (2018). A first assessment of the Sentinel-2 Level 1-C cloud mask product to support informed surface analyses. *Remote sensing of environment*, *217*, 426-443.

Conradsen, K., Nielsen, A. A., Schou, J., & Skriver, H. (2003). A test statistic in the complex Wishart distribution and its application to change detection in polarimetric SAR data. *IEEE Transactions on Geoscience and Remote Sensing*, *41*(1), 4-19.

Conradsen, K., Nielsen, A. A., & Skriver, H. (2016). Determining the points of change in time series of polarimetric SAR data. *IEEE Transactions on Geoscience and Remote Sensing*, *54*(5), 3007-3024.

Corbari, C., Paciolla, N., Ben Charfi, I., & Woods, M. (2021, April). Remote Sensing and Citizen science supporting irrigation monitoring in the Capitanata Irrigation Consortium (Italy). In *EGU General Assembly Conference Abstracts* (pp. EGU21-13318).

Droogers, P., & Aerts, J. (2005). Adaptation strategies to climate change and climate variability: a comparative study between seven contrasting river basins. *Physics and Chemistry of the Earth, Parts A/B/C*, *30*(6-7), 339-346.

Enderle, D. I., & Weih Jr, R. C. (2005). Integrating supervised and unsupervised classification methods to develop a more accurate land cover classification. *Journal of the Arkansas Academy of Science*, *59*(1), 65-73.

ESA, E. (2013). Sentinel-2 User Handbook. *European Space Agency*.

Foody, G. M., & Mathur, A. (2004). Toward intelligent training of supervised image classifications: directing training data acquisition for SVM classification. *Remote Sensing of Environment*, *93*(1-2), 107-117

Foody, G. M. (2004). Thematic map comparison. *Photogrammetric Engineering & Remote Sensing*, *70*(5), 627-633.

Foucher, S., & López-Martínez, C. (2014). Analysis, evaluation, and comparison of polarimetric SAR speckle filtering techniques. *IEEE transactions on image processing*, *23*(4), 1751-1764

De Fraiture, C., & Giordano, M. (2014). Small private irrigation: A thriving but overlooked sector. *Agricultural Water Management*, *131*, 167-17.

Friedl, M. A., Woodcock, C., Gopal, S., Muchoney, D., Strahler, A. H., & Barker-Schaaf, C. (2000). A note on procedures used for accuracy assessment in land cover maps derived from AVHRR data.

Funk, C. C., & Brown, M. E. (2009). Declining global per capita agricultural production and warming oceans threaten food security. *Food Security*, *1*(3), 271-289.

Gao, B. C. (1996). NDWI—A normalized difference water index for remote sensing of vegetation liquid water from space. *Remote sensing of environment*, *58*(3), 257-266.

Gao, Q., Zribi, M., Escorihuela, M. J., Baghdadi, N., & Segui, P. Q. (2018). Irrigation mapping using Sentinel-1 time series at field scale. *Remote Sensing*, *10*(9), 1495.

Godfray, H. C. J., Beddington, J. R., Crute, I. R., Haddad, L., Lawrence, D., Muir, J. F., ... & Toulmin, C. (2010). Food security: the challenge of feeding 9 billion people. *science*, *327*(5967), 812-818.

Goodman, J. W. (1976). Some fundamental properties of speckle. *JOSA*, *66*(11), 1145-1150.

Hammond, T. O., & Verbyla, D. L. (1996). Optimistic bias in classification accuracy assessment. *International Journal of Remote Sensing*, *17*(6), 1261-1266.

Hardisky, M., Klemas, V., & Smart, M. (1983). The influence of soil salinity, growth form, and leaf moisture on the spectral radiance of. *Spartina alterniflora*, *49*, 77-83

He, H., & Garcia, E. A. (2009). Learning from imbalanced data. *IEEE Transactions on knowledge and data engineering*, *21*(9), 1263-1284.

Hoekman, D. H., & Bouman, B. A. M. (1993). Interpretation of C-and X-band radar images over an agricultural area, the Flevoland test site in the Agriscatt-87 campaign. *TitleREMOTE SENSING*, *14*(8), 1577-1594.

Hollander, V. (2018). Mapping of farmer-led irrigated agriculture with remote sensing: A case study in Central Mozambique.

Horning, N. (2010, December). Random Forests: An algorithm for image classification and generation of continuous fields data sets. In Proceedings of the International Conference on Geoinformatics for Spatial Infrastructure Development in Earth and Allied Sciences, Osaka, Japan (Vol. 911).

Ihuoma, S. O., & Madramootoo, C. A. (2017). Recent advances in crop water stress detection. *Computers and Electronics in Agriculture*, *141*, 267-275.

Jansen, L. J., Bagnoli, M., & Focacci, M. (2008). Analysis of land-cover/use change dynamics in Manica Province in Mozambique in a period of transition (1990–2004). *Forest Ecology and Management*, *254*(2), 308-326.

Jin, Z., Azzari, G., You, C., Di Tommaso, S., Aston, S., Burke, M., & Lobell, D. B. (2019). Smallholder maize area and yield mapping at national scales with Google Earth Engine. *Remote sensing of environment*, *228*, 115-128.

Joseph, A. T., van der Velde, R., O'neill, P. E., Lang, R., & Gish, T. (2010). Effects of corn on C-and L-band radar backscatter: A correction method for soil moisture retrieval. *Remote Sensing of Environment*, *114*(11), 2417-2430.

Karam, M. A., & Fung, A. K. (1989). Leaf-shape effects in electromagnetic wave scattering from vegetation.

Karam, M. A., Fung, A. K., Lang, R. H., & Chauhan, N. S. (1992). A microwave scattering model for layered vegetation. *IEEE Transactions on Geoscience and Remote Sensing*, *30*(4), 767-784.

Karthikeyan, L., Chawla, I., & Mishra, A. K. (2020). A review of remote sensing applications in agriculture for food security: Crop growth and yield, irrigation, and crop losses. *Journal of Hydrology*, 124905.

Kim, S. B., van Zyl, J., Dunbar, S., Njoku, E., Johnson, J., Moghaddam, M., ... & Tsang, L. (2012). SMAP L2 & L3 Radar Soil Moisture (Active) Data Products. *Jet Propulsion Laboratory: Pasadena, CA, USA*.

Lavender, S. and Lavender, A. (2015). Practical handbook of remote sensing. CRC Press.

Lebourgeois, V., Dupuy, S., Vintrou, É., Ameline, M., Butler, S., & Bégué, A. (2017). A combined random forest and OBIA classification scheme for mapping smallholder agriculture at different nomenclature levels using multisource data (simulated Sentinel-2 time series, VHRS and DEM). *Remote Sensing*, *9*(3), 259.

Mahdianpari, M., Salehi, B., Mohammadimanesh, F., Homayouni, S., & Gill, E. (2019). The first wetland inventory map of newfoundland at a spatial resolution of 10 m using sentinel-1 and sentinel-2 data on the google earth engine cloud computing platform. *Remote Sensing*, *11*(1), 43.

McDonald, A. J., Bennett, J. C., Cookmartin, G., Crossley, S., Morrison, K., & Quegan, S. (2000). The effect of leaf geometry on the microwave backscatter from leaves. *International Journal of Remote Sensing*, *21*(2), 395-400.

Mellor, A., Boukir, S., Haywood, A., & Jones, S. (2015). Exploring issues of training data imbalance and mislabelling on random forest performance for large area land cover classification using the ensemble margin. *ISPRS Journal of Photogrammetry and Remote Sensing*, *105*, 155-168.

Mourad, K. A., Hosseini, S. H., & Avery, H. (2020). The role of citizen science in sustainable agriculture. *Sustainability*, *12*(24), 10375.

Müller-Wilm, U. (2016). Sen2Cor Configuration and UserManual.

Nguyen, D. B., Gruber, A., & Wagner, W. (2016). Mapping rice extent and cropping scheme in the Mekong Delta using Sentinel-1A data. *Remote Sensing Letters*, *7*(12), 1209-1218.

Onojeghuo, A. O., Blackburn, G. A., Huang, J., Kindred, D., & Huang, W. (2018). Applications of satellite 'hyper-sensing'in Chinese agriculture: Challenges and opportunities. *International journal of applied earth observation and geoinformation*, *64*, 62-86.

Ozdogan, M., Yang, Y., Allez, G., & Cervantes, C. (2010). Remote sensing of irrigated agriculture: Opportunities and challenges. *Remote sensing*, *2*(9), 2274-2304.

Pageot, Y., Baup, F., Inglada, J., Baghdadi, N., & Demarez, V. (2020). Detection of irrigated and rainfed crops in temperate areas using Sentinel-1 and Sentinel-2 time series. *Remote Sensing*, *12*(18), 3044.

Piiroinen, R., Heiskanen, J., Mõttus, M., & Pellikka, P. (2015). Classification of crops across heterogeneous agricultural landscape in Kenya using AisaEAGLE imaging spectroscopy data. *International Journal of Applied Earth Observation and Geoinformation*, *39*, 1-8.

Rouse, J. W., Haas, R. H., Schell, J. A., Deering, D. W., & Harlan, J. C. (1974). Monitoring the vernal advancement and retrogradation (green wave effect) of natural vegetation. *NASA/GSFC Type III Final Report, Greenbelt, Md*, *371*.

Sarabandi, K., Senior, T. B., & Ulaby, F. T. (1988). Effect of curvature on the backscattering from a leaf. *Journal of Electromagnetic Waves and Applications*, *2*(7), 653-670.

Senior, T. B. A., Sarabandi, K., & Ulaby, F. T. (1987). Measuring and modeling the backscattering cross section of a leaf. *Radio Science*, *22*(06), 1109-1116.

Shi, W., Zhang, M., Zhang, R., Chen, S., & Zhan, Z. (2020). Change detection based on artificial intelligence: State-of-the-art and challenges. *Remote Sensing*, *12*(10), 1688.

Song, C., Woodcock, C. E., Seto, K. C., Lenney, M. P., & Macomber, S. A. (2001). Classification and change detection using Landsat TM data: when and how to correct atmospheric effects?. *Remote sensing of Environment*, *75*(2), 230-244.

SNAP (2018). ESA Sentinel Application Platformv6.0.0.

Steele-Dunne, S. C., McNairn, H., Monsivais-Huertero, A., Judge, J., Liu, P. W., & Papathanassiou, K. (2017). Radar remote sensing of agricultural canopies: A review. *IEEE Journal of Selected Topics in Applied Earth Observations and Remote Sensing*, *10*(5), 2249-2273.

Talebi, H., Peeters, L. J., Otto, A., & Tolosana-Delgado, R. (2021). A Truly Spatial Random Forests Algorithm for Geoscience Data Analysis and Modelling. *Mathematical Geosciences*, 1-22.

Timothy A Warner, Giles M Foody, and M Duane Nellis. The SAGE handbook of remote sensing. Sage Publications, 2009.

Thenkabail, P. S., Schull, M., & Turral, H. (2005). Ganges and Indus river basin land use/land cover (LULC) and irrigated area mapping using continuous streams of MODIS data. *Remote Sensing of Environment*, *95*(3), 317-341.

Turral, H., Burke, J., & Faurès, J. M. (2011). *Climate change, water and food security* (No. 36). Food and Agriculture Organization of the United Nations (FAO).

Ulaby, F. (1975). Radar response to vegetation. *IEEE Transactions on Antennas and Propagation*, *23*(1), 36-45

Ulaby, F. T., Dubois, P. C., & Van Zyl, J. (1996). Radar mapping of surface soil moisture. *Journal of hydrology*, *184*(1-2), 57-84

Useya, J., & Chen, S. (2019). Exploring the Potential of Mapping Cropping Patterns on Smallholder Scale Croplands Using Sentinel-1 SAR Data. *Chinese Geographical Science*, *29*(4), 626-639.

United Nations. World population prospects 2019: Highlights, 2019. URL https://population.un.org/wpp/Publications/Files/WPP2019_Highlights.pdf. (accessed on 17 November 2020).

Virnodkar, S. S., Pachghare, V. K., Patil, V. C., & Jha, S. K. (2020). Remote sensing and machine learning for crop water stress determination in various crops: a critical review. *Precision Agriculture*, *21*(5), 1121-1155.

Vogels, M. F. A. (2019). Monitoring smallholder irrigation using remote sensing and object-based image analysis: Case studies in Eastern Africa (Doctoral dissertation, University Utrecht).

Vörösmarty, C. J., & Sahagian, D. (2000). Anthropogenic disturbance of the terrestrial water cycle. *Bioscience*, *50*(9), 753-765.

Warner, T. A., Foody, G. M., & Nellis, M. D. (2009). *The SAGE handbook of remote sensing*. Sage Publications.

Watkins, B., & Van Niekerk, A. (2019). A comparison of object-based image analysis approaches for field boundary delineation using multi-temporal Sentinel-2 imagery. Computers and Electronics in Agriculture, 158, 294-302.

Wu, M., Huang, W., Niu, Z., Wang, Y., Wang, C., Li, W., ... & Yu, B. (2017). Fine crop mapping by combining high spectral and high spatial resolution remote sensing data in complex heterogeneous areas. *Computers and Electronics in Agriculture*, *139*, 1-9.

Yueh, S. H., Kong, J. A., Jao, J. K., Shin, R. T., & Le Toan, T. (1992). Branching model for vegetation. *IEEE Transactions on Geoscience and Remote Sensing*, *30*(2), 390-402.

Zhen, Z., Quackenbush, L. J., Stehman, S. V., & Zhang, L. (2013). Impact of training and validation sample selection on classification accuracy and accuracy assessment when using reference polygons in object-based classification. *International Journal of Remote Sensing*, *34*(19), 6914-6930.

Appendix A

Spatial distribution of training polygons

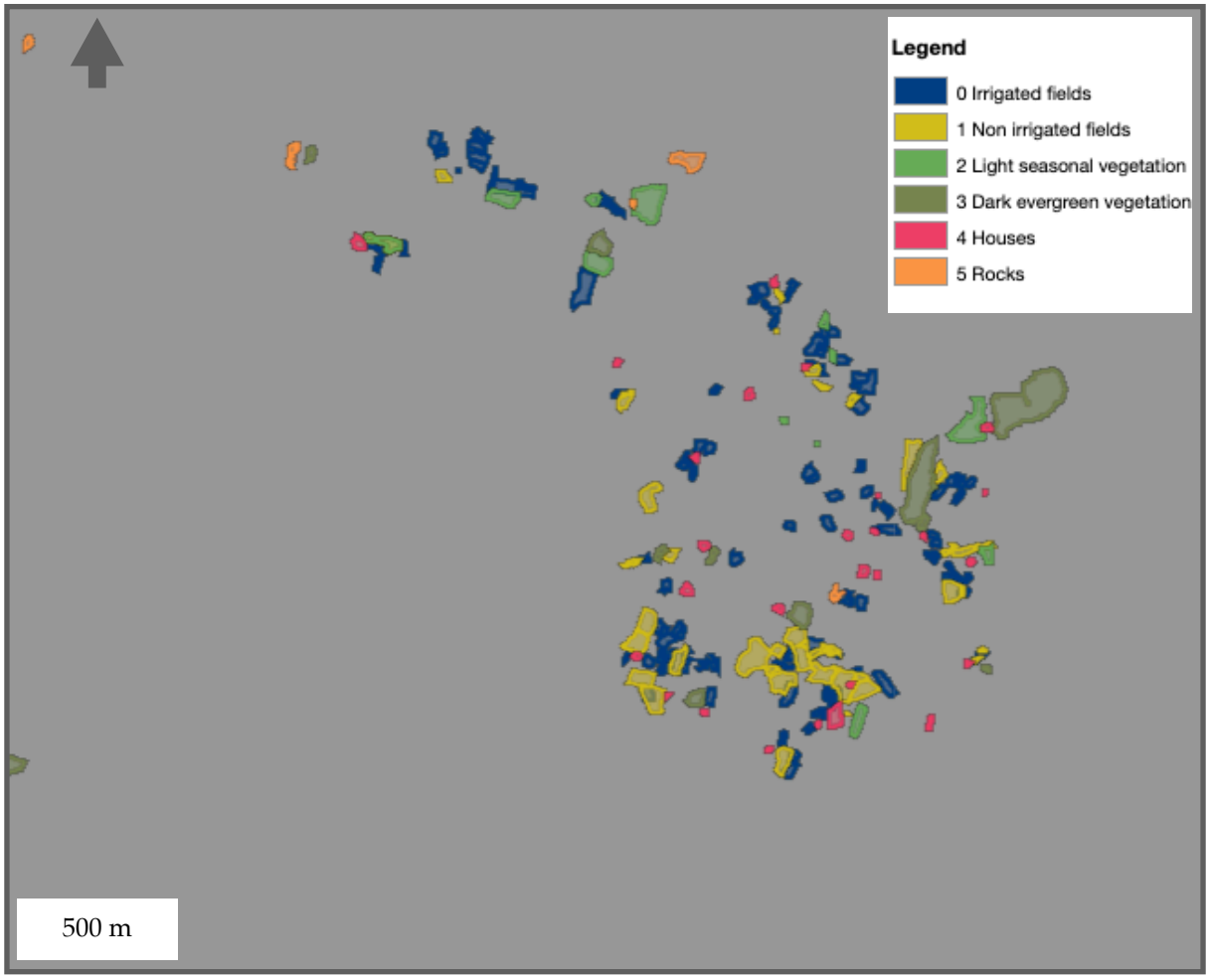

Figure A.1. Spatial distribution of training polygons.

Size of polygons of different land classed compared irrigated fields

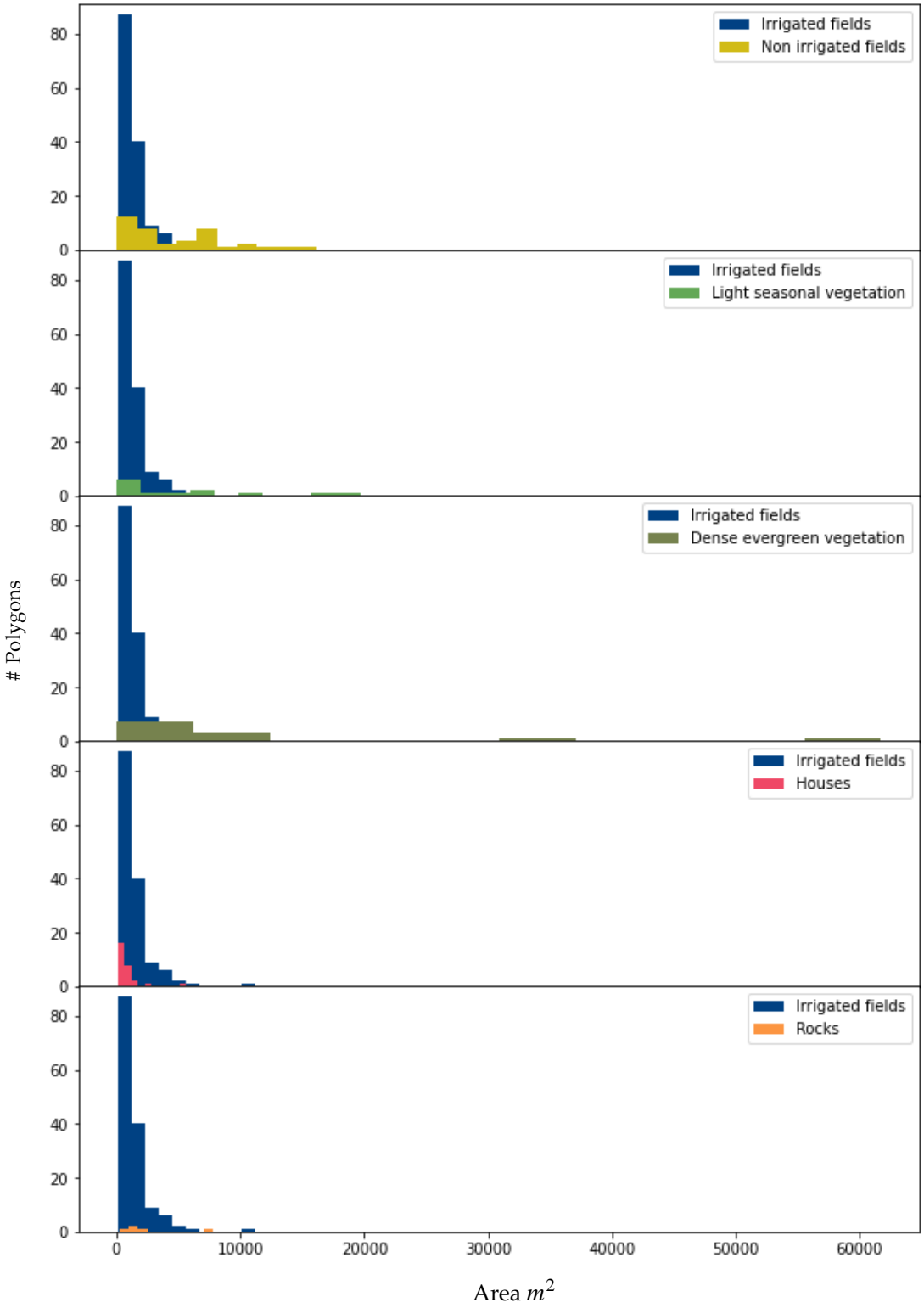

Figure A.2. Size of polygons of different land classed compared to irrigated fields.

Appendix B

Google Earth Engine provides level-1 ground range detected (GRD) products are multi-looked and ground range detected images that are converted to decibels. The mathematical processes to obtain these backscatter signals with the provided product are described here.

Single look comple SAR

The Sentinel-1 dual polarimetric synthetic aperture system emits radar microwaves in the C-band. These microwaves consist of one polarization, mainly vertical, and recieves both vertical and horizontal reflected polarizatios. Mathematically, this is represented as:

$$\begin{pmatrix} E_v^b \\ E_h^b \end{pmatrix} = \frac{e^{-irk}}{r} \begin{pmatrix} S_{vv} S_{vh} \\ S_{hv} S_{hh} \end{pmatrix} \begin{pmatrix} E_v^i \\ 0 \end{pmatrix}$$

The backscatter signal:

$$\begin{pmatrix} E_v^b \\ E_h^b \end{pmatrix}$$

is composed of the following components: the incident and vertically polarized radar signal:

$$\begin{pmatrix} E_v^i \\ 0 \end{pmatrix}$$

that is transformed by a complex scattering matrix:

$$\begin{pmatrix} S_{vv} & S_{vh} \\ S_{hv} & S_{hh} \end{pmatrix}$$

The exponent term accounts for the phase shift which is the consequence of the return distance r from the target to the sensor, where k is the wave number representing $k = 2\pi/\lambda$. Two out of four complex scattering matrix elements can be derived from measurements of the sensors backscattered radiation. These two complex scattering matrix elements can be processed into 2D arrays, consisting of the slant range x azimuth and represent the single look complex image.

The single look complex image can be written as a complex vector with the two derived elements:

$$S = \begin{pmatrix} S_{vv} \\ S_{vh} \end{pmatrix}.$$

The complex transpose S^T of the vector S is written as $(S_{vv}^* \; S_{vh}^*)$ where * stands for the complex conjugation. The span image or inner product of S denotes the total power:

$$P = S^T S = (S_{vv}^* S_{vh}^*) \begin{pmatrix} S_{vv} \\ S_{vh} \end{pmatrix} = |S_{vv}|^2 + |S_{vh}|^2$$

The covariance matrix image or the outer productes is denoted as:

$$C2 = SS^T = (S_{vv}^* S_{vh}^*) \begin{pmatrix} S_{vv} \\ S_{vh} \end{pmatrix} = \begin{pmatrix} |S_{vv}|^2 S_{vv}^* S_{vh} \\ S_{vh}^* S_{vv} |S_{vh}|^2 \end{pmatrix}$$

The elements on the diagonal are real numbers. The off-diagonal elements are the complex conjugates of each other and depict the relative phases of S_{vv} and S_{vh}. Since the off-diagonal images are not available in GEE, the representation of covariance matrix is:

$$C2 = \begin{pmatrix} |S_{vv}|^2 0 \\ 0 |S_{vh}|^2 \end{pmatrix}$$

Written in radar scattering cross sections:

$$\sigma^0 = C2 = \frac{1}{4\pi}\begin{pmatrix} \sigma^o_{vv}0 \\ 0\sigma^0_{vh} \end{pmatrix}$$

Speckle effects

One of the difficulties in handling SAR data is the presence of speckle effects that make visual interpretation challenging. In pictures, the speckle effect appears as random noise but is in fact a consequence of the coherent nature of the radar signal. The SLC signal, for a single vv polarization can be modelled in the form:

$$S_{vv} = \frac{|S^a_{vv}|}{\sqrt{n}} \sum_{k=1}^{n} e^{-i\phi_k}$$

$|S^a_{vv}|$ Represents the overall amplitude. This is constructed from the signal that is scattered from an area of one signal pixel. In this study, a pixel with a size of $10x10$ m^2 is used. The phase is set equal to 0. When the signal interacts with the target in the irratiated area, a part of the signal is randomly scattered. These randomly distributed scatterers add coherently and causes a phase change in the received signal. This phase change is included in the sum part of the above described equation and causes speckle effects. The intensity of these speckle effects varies from pixel to pixel.

The decomposed equation shows the real and the imaginary part:

$$S_{vv} = \frac{|S^a_{vv}|}{\sqrt{n}} \sum_{k=1}^{n} e^{-i\phi_k} = \frac{|S^a_{vv}|}{\sqrt{n}}\left(\sum_k cos\phi_k + \boldsymbol{i}\sum_k sin\phi_k\right) = \frac{|S^a_{vv}|}{\sqrt{n}}(x + \boldsymbol{i}y)$$

$$x = cos\phi_k, y = sin\phi_k$$

The ϕ_k denotes the phase shifts. ϕ_k Are both randomly and uniformly distributed and therefore present the variables x and y the sums of the cosine and sine terms, that are identically distributed.

If these conditions are me and according to the central limit theorem of statistics, x and y will have a normal distribution with zero mean and a variance of $\sigma^2 = n/2$, within the limit of a large number of n scatterers. In the expression for covariance of x and y, the sum of products of the cosine and sine term cancel to 0. This means that x and y are uncorrelated and consequently, $x + \boldsymbol{i}y$ and the SLC signal S_{vv} has a complex normal distribution. The pixel values of the vv intensity images are given by the square of the amplitude of S_{vv}:

$$|S_{vv}|^2 = S_{vv}S_{vv}^* = \frac{|S_{vv}^a|}{n})(x^2 + y^2)$$

Multi look SAR

Multi-look processing is done by averaging adjacent pixels for the purpose of reducing the effect of speckle and to compress the data. This averaging takes places in the frequency domain and not in the spatial domain. However, the process of multi-look averaging is at the expense of the spatial resolution. The spatial resolution is a characteristic of the sensor that determines the distance at which he can recognise adjacent objects. Pixel spacing indicates the distance in meters between neighbouring pixels in an image.

The Sentinel-1 interferometric wide swath mode consist of pixels of $20x4\ m^2$ that respresent the azimuth x range. During multi-looking processing, the average of five cells is taken in the direction of the range to accomplish a $20x20\ m^2$ resolution and then resampled to $10x10\ m^2$.

The formula can also be written as:

$$|S_{vv}|^2 = \frac{|S_{vv}^a|}{n}\frac{n}{2}(\frac{x^2}{n/2} + \frac{y^2}{n/2}) = |S_{vv}|^2\frac{u}{2}$$

$$u = (\frac{x^2}{n/2} + \frac{y^2}{n/2})$$

The latter denotes the sum of the squares of two variables.

Appendix C

Confusion matrix of training data set of red-edge bands in IS-2

Training matrix irrigation season 2 red-edge bands

	IF	NIF	LV	DV	H	R	PA%
IF	1701	13	0	0	0	0	99.5
NIF	36	1536	12	1	0	0	97.1
LV	2	33	583	0	0	0	93.3
DV	0	0	1	1124	0	0	99.8
H	2	2	0	0	205	0	98.6
R	0	0	0	0	0	105	100
UA%	97.7	97.3	98.1	99.9	100	100	98.1

Table C.1. Training and testing accuracy of RF (100) based on RE bands, from both irrigation seaon 2, κ is 97.5%.

Confusion matrix of testing data set of red-edge bands in IS-2

Training matrix irrigation season 1 red-edge bands-1

	IF	NIF	LV	DV	H	R	PA%
IF	1708	10	1	0	0	0	99.4
NIF	37	1539	1	0	0	0	97.6
LV	1	40	574	0	0	0	93.3
DV	0	1	2	1103	0	0	99.7
H	1	3	0	0	204	0	98.1
R	0	0	0	0	0	100	100
UA%	97.7	96.9	98.8	99.9	100	100	98.2

Table C.2. Training and testing accuracy of RF (100) based on RE bands, from both irrigation seaons, κ is 97.6%.